

**ISTANBUL TECHNICAL UNIVERSITY ★ GRADUATE SCHOOL OF SCIENCE**  
**ENGINEERING AND TECHNOLOGY**

**PRODUCTION AND CHARACTERIZATION OF TiO<sub>2</sub> NANOTUBES ON CP  
TITANIUM SURFACE**

**M.Sc. THESIS**

**Timur ÖZTÜRK**

**Department of Metallurgical and Materials Engineering**

**Materials Engineering Programme**

**JANUARY 2012**



**ISTANBUL TECHNICAL UNIVERSITY ★ GRADUATE SCHOOL OF SCIENCE**  
**ENGINEERING AND TECHNOLOGY**

**PRODUCTION AND CHARACTERIZATION OF TiO<sub>2</sub> NANOTUBES ON CP  
TITANIUM SURFACE**

**M.Sc. THESIS**

**Timur ÖZTÜRK**  
**(506091444)**

**Department of Metallurgical and Materials Engineering**

**Materials Engineering Programme**

**Thesis Advisor: Assoc. Prof. Dr. Murat BAYDOĞAN**

**JANUARY 2012**



**İSTANBUL TEKNİK ÜNİVERSİTESİ ★ FEN BİLİMLERİ ENSTİTÜSÜ**

**CP TİTANYUM YÜZEYİNDE TiO<sub>2</sub> NANOTÜP OLUŞUMU VE  
KARAKTERİZASYONU**

**YÜKSEK LİSANS TEZİ**

**Timur ÖZTÜRK  
(506091444)**

**Metalurji ve Malzeme Mühendisliği Anabilim Dalı**

**Malzeme Mühendisliği Programı**

**Tez Danışmanı: Doç. Dr. Murat BAYDOĞAN**

**OCAK 2012**



**Timur Öztürk**, a **M.Sc.** student of ITU **Institute of Science and Technology** student ID **506091444** successfully defended the **thesis** entitled “**PRODUCTION AND CHARACTERIZATION OF TiO<sub>2</sub> NANOTUBES ON CP TITANIUM SURFACE**”, which he prepared after fulfilling the requirements specified in the associated legislations, before the jury whose signatures are below.

**Thesis Advisor :**      **Assoc. Prof. Dr. Murat BAYDOĞAN**      .....  
Istanbul Technical University

**Jury Members :**      **Prof. Dr. Hüseyin ÇİMENOĞLU**      .....  
Istanbul Technical University

**Assist. Prof. Dr. Erdem ATAR**      .....  
Gebze Institute of Technology

**Date of Submission : 19 December 2011**

**Date of Defense : 26 January 2012**





*To my family,*



## **FOREWORD**

Among many people I have to thank, my thesis advisor Assoc. Prof. Dr. Murat BAYDOĞAN has a very special place. This endeavour would not be achievable without his guidance, support and motivating approach throughout my graduate studies. I would also like to thank Prof. Dr. Eyüp Sabri KAYALI and Prof. Dr. Hüseyin ÇİMENOĞLU, for their guidance and supports that they displayed from the first day of my undergraduate education.

I also would like to express my thanks to Res. Assist. Onur MEYDANOĞLU for his assistance in my laboratory studies and helps during my graduate education.

I wish my best opinions to Mert GÜNYÜZ, Hakan KARAKAFA, Res. Assist. Hasan GÖKÇE, Ph. D. student Aziz GENÇ and Hüseyin SEZER for their helps to complete the characterization works of experiments in laboratories.

Finally, I especially thank my family for giving me support when needed in my whole life.

January 2012

Timur ÖZTÜRK  
Materials Engineer



## TABLE OF CONTENTS

	<u>Page</u>
<b>FOREWORD</b> .....	<b>ix</b>
<b>TABLE OF CONTENTS</b> .....	<b>xi</b>
<b>ABBREVIATIONS</b> .....	<b>xiii</b>
<b>LIST OF TABLES</b> .....	<b>xv</b>
<b>LIST OF FIGURES</b> .....	<b>xvii</b>
<b>SUMMARY</b> .....	<b>xix</b>
<b>ÖZET</b> .....	<b>xxi</b>
<b>1. INTRODUCTION</b> .....	<b>1</b>
<b>2. TITANIUM AND TITANIUM ALLOYS</b> .....	<b>3</b>
2.1 CP (Commercially Pure) Titanium .....	4
2.2 Titanium Alloys.....	8
2.3 Physical Properties .....	9
2.4 Oxidation of Titanium.....	11
2.5 Crystal Structure.....	11
<b>3. NANOSTRUCTURED MATERIALS</b> .....	<b>13</b>
3.1 Nanotubes.....	14
3.1.1 Carbon nanotubes.....	15
3.1.2 Metal chalcogenide nanotubes .....	17
3.1.3 Metal oxide nanotubes .....	19
<b>4. TITANIUM DIOXIDE NANOTUBES</b> .....	<b>21</b>
4.1 Synthesis Techniques .....	21
4.1.1 Template methods .....	22
4.1.2 Alkaline hydrothermal synthesis of elongated titanates .....	22
4.1.3 Anodic oxidation.....	24
4.2 Applications of Titanium Dioxide Nanotubes.....	25
<b>5. THE ELECTROCHEMICAL ANODIZATION PROCESS</b> .....	<b>27</b>
5.1 Effect of Cathode Materials .....	28
5.2 Anodic Oxidation of Titanium .....	29
5.2.1 Mechanism of nanotube growth.....	30
<b>6. EXPERIMENTAL STUDIES</b> .....	<b>35</b>
6.1 Surface Preparation .....	36
6.2 Anodic Oxidation .....	36
6.3 Heat Treatment .....	37
6.4 Characterization Tests .....	38
6.4.1 X-ray diffraction analyses .....	38
6.4.2 Scanning electron microscope examinations .....	38
6.4.3 Contact angle measurements.....	39
6.4.4 Surface roughness measurements .....	40
<b>7. RESULTS AND DISCUSSION</b> .....	<b>41</b>
7.1 Surface Morphologies of Titanium Dioxide Nanotubes .....	41

7.1.1 Effect of voltage and time on nanotube diameter .....	41
7.1.2 Wall thickness variation .....	47
7.2 Structural Analysis of Titanium Dioxide Nanotubes .....	48
7.2.1 XRD patterns of unannealed samples .....	48
7.2.2 XRD patterns of annealed samples .....	50
7.3 Analysis of Contact Angle Measurements .....	51
7.4 Analysis of Surface Roughness Measurements.....	53
7.5 Evaluation of TiO <sub>2</sub> Nanotube Structures for Selected Applications .....	54
<b>8. CONCLUSIONS AND RECOMMENDATIONS .....</b>	<b>59</b>
<b>REFERENCES .....</b>	<b>61</b>
<b>APPENDICES .....</b>	<b>65</b>
APPENDIX A.1 .....	66
<b>CURRICULUM VITAE.....</b>	<b>77</b>

## **ABBREVIATIONS**

<b>ASM</b>	: American Society for Metals
<b>BCC</b>	: Body Centered Cubic
<b>CNT</b>	: Carbon Nanotube
<b>CP</b>	: Commercially Pure
<b>DC</b>	: Direct Current
<b>DI</b>	: Deionized Water
<b>DNA</b>	: Deoxyribonucleic Acid
<b>FESEM</b>	: Field Emission Scanning Electron Microscope
<b>HCP</b>	: Hexagonal Close Packed
<b>HRB</b>	: Hardness Rockwell B
<b>MWCN</b>	: Multi Walled Carbon Nanotube
<b>PEC</b>	: Photoelectrochemical Cell
<b>SEM</b>	: Scanning Electron Microscope
<b>SWCN</b>	: Single Walled Carbon Nanotube
<b>UV</b>	: Ultraviolet
<b>XRD</b>	: X-Ray Diffraction





## LIST OF TABLES

	<u>Page</u>
<b>Table 2.1</b> : CP titanium and important commercial titanium alloys .....	5
<b>Table 2.2</b> : Chemical composition and yield strength values for CP titanium and $\alpha$ titanium alloys. ....	7
<b>Table 2.3</b> : Properties of titanium metal at room temperature .....	10
<b>Table 3.1</b> : Summary of the inorganic nanotubes reported in literature and the synthetic procedures used for their production. ....	18
<b>Table 5.1</b> : Cathode materials used in TiO <sub>2</sub> anodization.....	28
<b>Table 6.1</b> : Annealing conditions applied to anodized CP titanium foils.....	37



## LIST OF FIGURES

	<u>Page</u>
<b>Figure 2.1</b> : Schematic product life cycle curve of some materials, with respect to various technologies on curve .....	4
<b>Figure 2.2</b> : Pseudo-binary section through a $\beta$ isomorphous phase diagram .....	8
<b>Figure 2.3</b> : Unit cell of (a) $\alpha$ and (b) $\beta$ phases .....	12
<b>Figure 3.1</b> : Structures with different sizes and aspects .....	14
<b>Figure 3.2</b> : Images of (a) SWNT and (b) MWNT .....	16
<b>Figure 3.3</b> : Simulation of a large-amplitude transverse deformation of a carbon nanotube.....	17
<b>Figure 3.4</b> : SEM images of (a) $\text{MnO}_2$ , (b) $\text{VO}_x$ , (c) $\text{ZrO}_2$ , (d) $\text{WS}_2$ , (e) $\text{Ni}_3\text{Si}_2\text{O}_5(\text{OH})_4$ and (f) $\text{Mg}_3\text{Si}_2\text{O}_5(\text{OH})_4$ nanotubes .....	19
<b>Figure 4.1</b> : Top-down and bottom-up approaches for $\text{TiO}_2$ nanomaterials .....	21
<b>Figure 4.2</b> : Template method for the preparation of nanostructured materials .....	22
<b>Figure 4.3</b> : TEM images of (a) and (c) titanate nanotubes, (b) and (d) nanofibres, (e) multilayer nanosheets and a SEM image of (f) an agglomerate of titanate nanotubes produced by alkaline hydrothermal treatments.....	24
<b>Figure 4.4</b> : Typical SEM images of $\text{TiO}_2$ nanotube arrays.....	25
<b>Figure 4.5</b> : Photocatalytic processes: (a) initial photocatalytic reactions and (b) the process of photochemical water splitting on $\text{TiO}_2$ nanotubes ....	26
<b>Figure 5.1</b> : Schematic view of an electrochemical cell in which titanium samples (anode) are anodized with the help of platinum cathode .....	27
<b>Figure 5.2</b> : Current - Time curve. (a) oxide barrier formation, (b) pores start to grow, (c) steady state of nanotube growth.....	31
<b>Figure 5.3</b> : Illustration of nanotube formation at constant anodization voltage. (a) Oxide layer formation, (b) pit formation, (c) growth of pits into pores, (d) oxidation and field assisted dissolution, (e) nanotubes .....	33
<b>Figure 6.1</b> : Flow chart of experimental procedure.....	35
<b>Figure 6.2</b> : Anodic oxidation equipment used in this study .....	37
<b>Figure 6.3</b> : Bruker X-Ray Diffractometer .....	38
<b>Figure 6.4</b> : JEOL JSM 7000F Field Emission Scanning Electron Microscope.....	39
<b>Figure 6.5</b> : KSV Cam 200 Contact Angle and Surface Tension Meter.....	39
<b>Figure 7.1</b> : SEM images of $\text{TiO}_2$ structures anodized at 10V for (a) 5 min, (b) 10 min, (c) 20 min and (d) 40 min .....	42
<b>Figure 7.2</b> : SEM images of $\text{TiO}_2$ structures anodized at 20V for (a) 5 min, (b) 10 min, (c) 20 min and (d) 40 min .....	43
<b>Figure 7.3</b> : SEM images of $\text{TiO}_2$ structures anodized at 40V for (a) 5 min, (b) 10 min, (c) 20 min and (d) 40 min .....	44
<b>Figure 7.4</b> : Surface morphologies of samples anodized at (a) 10V for 40 minutes and (b) 40V for 5 minutes .....	45
<b>Figure 7.5</b> : Variation of average nanotube diameter with anodization time.....	45
<b>Figure 7.6</b> : Typical current density - anodization time diagram.....	46

<b>Figure 7.7 :</b> Current density - anodization time diagram of sample anodized at 10V for 10 minutes .....	47
<b>Figure 7.8 :</b> SEM images showing wall thickness of titanium dioxide nanotubes for samples anodized at 10V for (a) 10 min and (b) 20 min.....	48
<b>Figure 7.9 :</b> XRD pattern of titanium foil anodized at 10V for 10 minutes .....	49
<b>Figure 7.10 :</b> XRD pattern retrieved from literature .....	49
<b>Figure 7.11 :</b> XRD pattern of sample annealed at 480°C for 24 hours .....	50
<b>Figure 7.12 :</b> View of a water droplet 10s after dropped on CP titanium sample anodized at 10V for 10 minutes.....	51
<b>Figure 7.13 :</b> Contact angle measurements of samples anodized at 10V as a function of anodization time .....	52
<b>Figure 7.14 :</b> Contact angle measurements of samples anodized at 20V as a function of anodization time .....	52
<b>Figure 7.15 :</b> Contact angle measurements of samples anodized at 40V as a function of anodization time .....	53
<b>Figure 7.16 :</b> Variation of mean surface roughness as a function of anodization time for different anodization voltages .....	54
<b>Figure 7.17 :</b> Schematic representation of crystallization steps of TiO <sub>2</sub> nanotubes..	55
<b>Figure 7.18 :</b> Schematic representation of PEC .....	57
<b>Figure A.1 :</b> XRD patterns of unannealed samples anodized at 10V with anodization time: (a) 5 minutes, (b) 10 minutes, (c) 20 minutes, (d) 40 minutes .....	67
<b>Figure A.2 :</b> XRD patterns of unannealed samples anodized at 20V with anodization time: (a) 5 minutes, (b) 10 minutes, (c) 20 minutes, (d) 40 minutes .....	69
<b>Figure A.3 :</b> XRD patterns of unannealed samples anodized at 40V with anodization time: (a) 5 minutes, (b) 10 minutes, (c) 20 minutes, (d) 40 minutes .....	71
<b>Figure A.4 :</b> XRD patterns of samples annealed at 480°C. Annealing time: (a) 1 hour, (b) 2 hours, (c) 4 hours, (d) 8 hours, (e) 24 hours, (f) 48 hours.....	73
<b>Figure A.5 :</b> XRD patterns of samples annealed at (a) 400°C for 1 hour, (b) 500°C for 1 hour, (c) 600°C for 1 hour, (d) 600°C for 60 hours, (e) 700°C for 1 hour .....	75

## **PRODUCTION AND CHARACTERIZATION OF TiO<sub>2</sub> NANOTUBES ON CP TITANIUM SURFACE**

### **SUMMARY**

Titanium and its alloys have very high strength to weight ratio, good mechanical properties, high corrosion resistance and adaptability to be used as biomaterials. With this variety of applications, they are available for various applications. Moreover, recent researches in the last decade added another dimension to titanium's versatility; nanoscale applications. With the help of nanoscale structure on titanium surface, better control of surface related applications became possible.

In this study, production of highly ordered and vertically oriented titanium dioxide nanotube layers by anodization of CP titanium foils and the effect of annealing on nanotube structures were investigated. Experimental works consisted of four main steps including surface preparation of CP titanium, anodic oxidation of samples, annealing of anodized samples and characterization works before and after annealing. Anodic oxidation was performed in an aqueous solution of 1% HF. CP titanium foil was used as anode, while platinum wire was used as cathode. Regular arrangements of the nanotubes were obtained on the sample anodized at 10V for 10 minutes and then this sample was annealed. The aim of annealing, which was performed at 400°C to 700°C for various times, is to transform amorphous structure of as anodized sample into crystalline structure comprising anatase and rutile modification of TiO<sub>2</sub>.

Structural and morphological characterization works of anodized and annealed samples were studied by qualitative X-Ray diffraction (XRD) analyses, scanning electron microscope (SEM) examinations, contact angle and surface roughness measurements.

Experimental results were evaluated on the basis of anodization voltage and time and annealing temperature and time. XRD patterns of as anodized samples showed that only  $\alpha$  titanium peaks coming from the underlying titanium. Nanotube morphology as well as nanotube diameter and wall thickness were examined by SEM. It was observed that increasing anodization voltage has a deteriorating effect on nanotube morphology of the samples. Nanotube morphology was clearly observed on the surface of the samples anodized at 10V, while this morphology seem to be started to deteriorate on the samples anodized at 20V, and finally surface has an etched like appearance for the samples anodized at 40V. It was also shown that anodization time has no significant effect on nanotube morphology on the samples anodized at 10V and 20V. When the anodization voltage is increased to 40V, surface becomes increasingly deteriorated with increasing anodization time.

Contact angle measurement provides some information about the wettability of surfaces, which is especially important to evaluate biomedical applications of the surface. Contact angle measurements showed that, contact angle decreased with

increasing anodization voltage. Mean surface roughness, on the other hand, increased with increasing anodization potential, which is in agreement with the results of contact angle measurements in that surfaces with higher roughness exhibited lower contact angle values.

Based on the results of characterization works, optimum anodization parameters (voltage and time) were determined as 10V for 10 minutes, respectively, to produce a regular arranged nanotube arrays on CP titanium.

In addition, obtained experimental results were also evaluated to discuss the availability of the produced nanotube structure for hydrogen sensing and photocatalysis applications.

## CP TİTANYUM YÜZEYİNDE TiO<sub>2</sub> NANOTÜP OLUŞUMU VE KARAKTERİZASYONU

### ÖZET

Titanyum ve alaşımları çok yüksek mukavemet – ağırlık oranına, iyi mekanik özelliklere, üstün korozyon direncine ve biyomalzeme uygulamalarına yatkınlıkları sayesinde çok çeşitli alanlarda kullanım imkânı bulmaktadır. Teknolojinin her geçen gün ilerlemesiyle artan araştırma konuları sayesinde titanyum da nanoteknoloji alanında araştırma konusu olmuştur. Özellikle son on yılda yapılan çalışmalarla, titanyumun nano boyutlu uygulamalarda da kullanılabilceği saptanmıştır. Titanyum yüzeyinde yapılabilen nano ölçekteki modifikasyonlar sayesinde yüksek yüzey alanı gerektiren çalışmaların önü açılmış ve titanyumun metalinin genel özelliklerinin yanı sıra, mevcut kullanım alanlarından farklı alanlarda da titanyumdan faydalanılabileceği ispatlanmıştır.

İlk olarak 1998 yılında yayınlanan bir makalede titanyum oksitli nano yapılardan bahsedilmiş, 2001 yılında ise titanyum dioksit nanotüplerin anodik oksidasyon yöntemi ile ilk kez başarılı bir şekilde sentezlenmesi hakkında yayın yapılmıştır. Anodik oksidasyonun önemi, yapıda kontrollü bir oksitlenme sağlayabilmektir ve bu sayede TiO<sub>2</sub> yapısı metal yüzeyinde elde edilmektedir. Elde edilen TiO<sub>2</sub> yapısının çok sayıda nano boyutlu tüpten oluşması ise elektroliti oluşturan kimyasalların özelliklerine, elektrolit/metal ara yüzeyinde oluşan reaksiyonlara, anodik oksidasyon esnasında uygulanan gerilime ve harcanan süreye bağlıdır. Bu bilgilerin ışığında yapılan araştırmalarla titanyum dioksit nanotüplerin hangi koşullarda üretilebileceği incelenmiş olup hidrojen sensörü, süper kapasitörler, güneş pilleri ve biyosensör olarak kullanımı ile ilaç taşınımı ve fotokataliz uygulamalarına yatkınlığı gibi pek çok alanda kullanılabilceği saptanmıştır.

Bu çalışmada, titanyum metalinin anodik oksidasyon ile üretilerek düzenli bir şekilde istiflenmiş titanyum dioksit nanotüp yüzeylerinin elde edilmesi ve ısıtma işleminin nanotüp yapılarına olan etkileri incelenmiştir. Deneysel çalışmalar, yüzey hazırlama, titanyumun anodik oksidasyonu, anodik oksidasyon yapılmış numunelerin tavlama ve tavlama yapılmadan önce ve sonra gerçekleştirilmiş karakterizasyon çalışmalarını içeren dört ana bölümden oluşmaktadır. Anodik oksidasyon işlemleri ortam koşullarında ve %1 HF içeren bir sulu elektrolit çözeltisinde gerçekleştirilmiştir. Ticari saflıktaki titanyum folyo anot olarak kullanılmış iken, katot malzemesi olarak yüksek iletkenliği ve anodik oksidasyon işlemlerine uygunluğu açısından platin tel kullanılmıştır.

Gerek sadece anodik oksidasyon yapılmış, gerekse de anodik oksidasyon sonrası tavlama işlemine de tabi tutulan numunelerin yapısal ve morfolojik karakterizasyonu, sırasıyla kalitatif X ışını difraksiyonu (XRD) analizi ve taramalı elektron mikroskobu (SEM) incelemeleri ile yapılmış, ayrıca anodik oksidasyon uygulanan örnekler üzerinde temas açısı ölçümü ve yüzey pürüzlülük ölçümleri yapılmıştır. Karakterizasyon işlemleri sonucunda elde edilen veriler ile düzenli ve homojen bir

nanotüp morfolojisini veren anodik oksidasyon koşulları belirlenmiş, ayrıca anodik oksidasyon sonrası amorf yapıda olan TiO<sub>2</sub> nanotüplerin anataz ve rutil fazlarını içeren bir yapıya dönüştürülmesi amacıyla yapılan tavlama işleminin sıcaklık ve süresinin nanotüp yapısına etkisi incelenmiştir.

Deneysel çalışmaların sonuçları, anodik oksidasyon voltaj ve süresi ile tavlama sıcaklık ve süresi esas alınarak değerlendirilmiştir. SEM ile yapılan yüzey incelemelerinde nanotüp yapılarının oluşup oluşmadığına dair gözlemler yapılmış olup, bu nanotüplerin çapları ve et kalınlıkları ölçülmüştür. Anodik oksidasyon işlemi esnasında artan voltajın titanyum dioksit nanotüpler üzerinde bozucu bir etkisi olduğu görülmüştür. 10V voltaj uygulanan tüm örneklerde iyi bir dizilime sahip nanotüp yapısının belirgin bir şekilde olduğu gözlenebilirken, 20V değerinde voltaj uygulanan numunelerde nanotüplerin bozunmaya başladığı gözlenmiş, voltaj değeri 40V olarak uygulandığında ise nanotüp yapılarının yerine dağlanmış bir yüzey morfolojisinin elde edildiği belirlenmiştir. Anodik oksidasyon süresinin etkisi ise 5 ile 40 dakika arasında incelenmiş olup 10V ve 20V voltaj değerlerinde, anodik oksidasyon süresinin nanotüp dizilimine önemli bir etkisi olmadığı görülmüştür. Ancak, bu çalışmada uygulanan en yüksek voltaj değeri olan 40V değerinde, nanotüp yapısının bozulduğu görülmüştür.

Tavlama aşamasında, öncelikle 480°C’de 1, 2, 4, 8 ve 24 saat süreyle tavlanan numunelerin yüzeylerinde yapısal olarak meydana gelen değişikliklerin belirlenmesi amacıyla XRD analizi yapılmıştır. Genel olarak bu sıcaklıkta tavlanan tüm numunelerde yapının anataz ve rutil fazları içerdiği belirlenmiş, ancak 8 saate kadar tavlanan numunelerde tavlama süresinin anataz ve rutil pik şiddetlerine belirgin bir etkisinin olmadığı gözlenmiştir. 480°C’de 24 saat süreyle yapılan tavlama sonucu ise her iki faza ait piklerin belirginleştiği görülmektedir. Daha sonra, tavlama sıcaklığının nanotüp yapısına etkisini görmek amacıyla, 10V’da 10 dakika süreyle anodik oksidasyon uygulanan numuneye, 400°C, 500°C, 600°C ve 700°C’de farklı süreler tavlama uygulanmıştır. Söz konusu tavlama numunelerine ait XRD paternlerinden, nispeten düşük sıcaklıklarda (400°C ve 500°C) anataz ve rutil fazlarının her ikisine ait pikler birlikte gözlenirken, tavlama sıcaklığı ya da süresi arttıkça rutil fazına ait piklerin artan şekilde şiddetlendiği görülmüştür. 700°C’de 1 saat süreyle yapılan tavlama sonrası ise yapıda sadece rutil fazına ait pikler gözlenmiştir.

Kapiler etki, sıvı ile katı yüzey arası yüzey geriliminin ölçülmesi açısından büyük önem taşımaktadır. Sıvı molekülleri arası çekim kuvvetlerinin meydana getirdiği kohezyon kuvvetleri ile sıvı – katı yüzey arasındaki çekim kuvvetleri yani adhezyon kuvvetleri, o malzemenin ıslanabilirliğini yani temas açısını belirler. Temas açısı ölçümleri, biyomedikal uygulamaları için önem taşıyan ıslanabilirlik hakkında bilgi vermektedir. Biyomedikal uygulamalarının yanı sıra, hidrojen sensörü uygulamaları ve ilaç emisyonuna yönelik uygulamalarda da ıslanabilirlik yani temas açısı büyük önem taşır ve bu özellik nanotüplerin gerek çapları ve dizilimleri gerekse de kristal yapıları ile doğrudan etkileşim içerisinde. Titanyum dioksit nanotüp yüzeyleri üzerinde yapılan temas açısı ölçümlerine göre, anodik oksidasyon voltajının artmasıyla, temas açısı değerlerinin azaldığı görülmektedir. Özellikle 40V değerinde anodik oksidasyon uygulanan numunelerde temas açısı değeri, temastan 10 saniye sonra yapılan ölçümlerde 70-75° olarak ölçülmüştür ve bu durum muhtemelen, taramalı elektron mikroskobu fotoğraflarından da görüldüğü gibi, bu numunelerde nanotüp yapısının büyük ölçüde bozulmasından kaynaklanmaktadır.



Ortalama yüzey pürüzlülüğü ölçümleri ile CP titanyum yüzeyinde oluşturulan nanotüp morfolojisinin yüzey pürüzlülüğüne etkisi incelenmiştir. Bu ölçümler ile ıslanabilirlik özelliği arasında ilişki kurulmuş ve TiO<sub>2</sub> nanotüplerin çeşitli uygulamalara elverişliliği araştırılmıştır. Yapılan ölçümlerden alınan sonuçlara göre, anodik oksidasyon esnasında uygulanan gerilimin şiddeti arttıkça numunelerin yüzey pürüzlülük değerlerinde de bununla orantılı olarak artışlar gözlenmektedir. Yüzeylerindeki nanotüp morfolojisinin bozulduğu numunelerin (40V voltaj altında anodik oksidasyon uygulanan numuneler) yüzey pürüzlülüğü değeri de en düşük olarak ölçülmüştür.

Karakterizasyon çalışmaları sonuçlarına göre, düzenli dizilime sahip optimum nanotüp morfolojisi elde etmek için gerekli anodik oksidasyon parametrelerinin (voltaj ve süre), 10V ve 10 dakika olduğu belirlenmiştir.

Elde edilen deneysel sonuçlar, üretilen nanotüp morfolojisinin hidrojen sensörü ve fotokataliz gibi uygulamalara uygunluğu bakımından da değerlendirilmiştir.



## 1. INTRODUCTION

Starting from its general production in 1940s, titanium increasingly became one of the most popular subjects in materials science in the late 20<sup>th</sup> century and still highly being studied on. With its versatile properties of high strength to weight ratio based on low density, excellent corrosion resistance and high melting point, titanium became the subject of numerous applications including chemical process industry, automotive industry, marine applications, aerospace materials and biomedical applications [1].

With an increase interest on nanoscience, titanium is studied in the purpose of having any characteristic property that cannot be observed on macro scale or different from other materials. Alongside its characteristic properties such as low weight and high strength, questions are asked by researchers; how can titanium be distinguished much more specifically? In order to investigate an answer for this question, further researches are studied on nanoscale.

First article about the synthesis of nanostructured titanates is published by Kasuga and co-workers in 1998 [2]. In the light of Kasuga and co-workers study, many attempts have been done to understand the mechanism of this nanoscale structures and finally first fabrication of titanium dioxide nanotubes (titania nanotubes) is achieved by anodization of titanium in 2001 by Gong and co-workers [3]. Significant developments occurred in titanium dioxide nanotubes research field with the approaches based on Gong's studies. Studies on titanium dioxide nanotubes and their properties are taking increasing interest of material scientists since these fabrication methods are successfully proven.

TiO<sub>2</sub> nanotube arrays have presented various properties which have a large number of diverse applications that include drug eluting surfaces, super capacitors, solid-state lithium batteries, hydrogen sensors, bio membranes and bio sensors, solar cells and photoelectrochemical cells for the solar generation of hydrogen [4].

Anodic oxidation or anodization, is one of the most versatile processes to produce highly ordered titanium dioxide nanotube arrays. Anodization of CP titanium in acidic electrolytes (especially fluoride containing ones) results in the fabrication of amorphous titanium dioxide nanotube arrays. In order to provide a transformation from amorphous to a crystalline state, annealing operation is applied to nanotube arrays generally in between 300°C and 550°C temperature range which is below fully rutile transformation temperature.

The aim of this study is to investigate the structure and properties of anodized titanium dioxide nanotubes and effect of heat treatment with the methods applied as mentioned above. After the fabrication of crystalline titanium dioxide nanotube arrays, results are reviewed for the availability of nanotube arrays for applications including hydrogen sensors and photocatalysis.

## 2. TITANIUM AND TITANIUM ALLOYS

Presumably, titanium is one of the most important and widely used of metals whose technology was developed in the second half of the 20th century. As well as being a strong and corrosion-resistant metal, titanium is also a very light metal with the relative density of  $4.50 \text{ g/cm}^3$ , that is nearly half of iron ( $7.87 \text{ g/cm}^3$ ), this gives it an excellent strength-to-weight ratio (which is also known as “specific strength”) at the same time. It is as corrosion-resistant as 18/8 stainless steel, but will also withstand the extreme corrosiveness of salt water. Titanium also has a melting point of  $1668^\circ\text{C}$ . It is this combination of high strength, low density and excellent corrosion resistance, which has led to the expansion of the use of titanium in the aerospace, chemical and engineering industries since the late 1940s. Titanium is now no longer a new metal but quite a commonly used metal [5].

Technological and industrial advancements covered in the titanium industry can be characterized by two main phases. The first phase was dominated by technical progress starting in the mid of 20th century and lasting until the mid-1980's [6]. The second and still continuing phase can be characterized by the transformation to a commercial industry when the technology was important but economics became a dominant consideration as a result of technological developments [7].

Today, with these technological progresses, titanium and its alloys are produced in a wide variety of product forms which are used in everyday life of human being. Titanium can be wrought, cast or made by powder metallurgy techniques and it may be joined by welding, brazing, adhesives, diffusion bonding or fasteners.

In Figure 2.1, a comparison between various materials can be seen. It is possible to figure out the effect of titanium production's toughness with respect to steel and aluminum. Researches indicate that, titanium is still in its growth era [8].

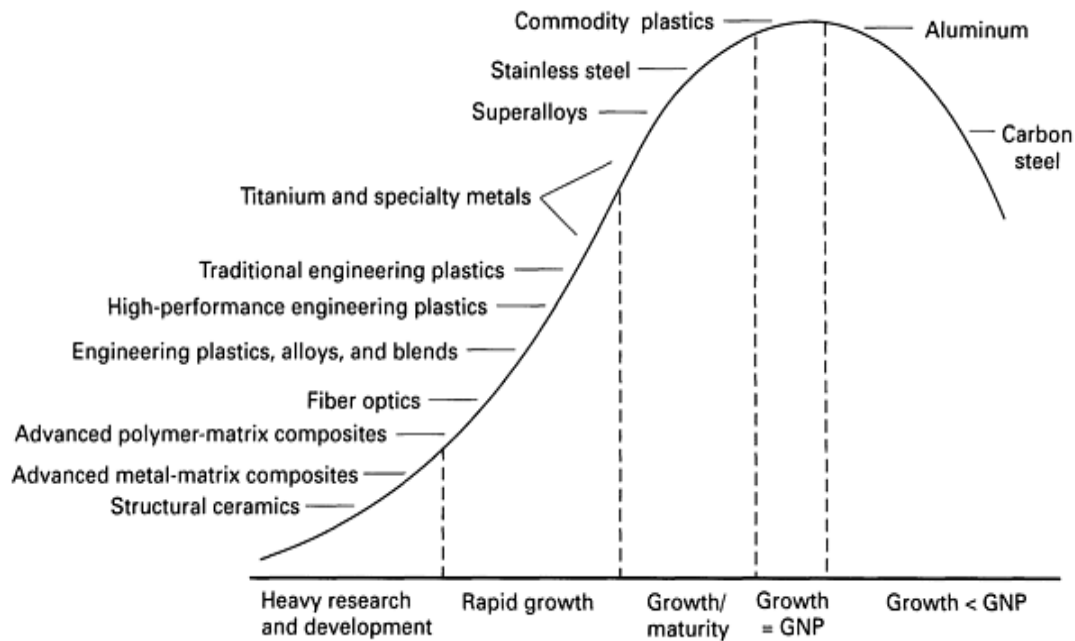


**Figure 2.1:** Schematic product life cycle curve of some materials, with respect to various technologies on curve [8].

## 2.1 CP (Commercially Pure) Titanium

Unalloyed titanium, generally known as commercially pure or commercial purity (CP) titanium is the weakest but most corrosion-resistant type of titanium metal. All  $\alpha$  titanium alloys are based on the hexagonal allotropic form of titanium at low temperature. These alloys can contain substitutional alloying elements (Al or Sn) or interstitial elements (oxygen, carbon, or nitrogen) which are soluble in the hexagonal  $\alpha$  phase. These alloys also contain some limited quantities of elements that have limited solubility such as iron (Fe), vanadium (V) and molybdenum (Mo). Table 2.1 lists a group of  $\alpha$  titanium alloys and grades of CP titanium, along with representative selections of alloys belonging to the  $\alpha+\beta$  and  $\beta$  classes [1].

**Table 2.1:** CP titanium and important commercial titanium alloys [1].

Common Name	Composition (% wt)	T <sub>β</sub> (°C)
<b>α Alloys and CP Titanium</b>		
Grade 1	CP-Ti (0.2 Fe, 0.18 O)	890
Grade 2	CP-Ti (0.3 Fe, 0.25 O)	915
Grade 3	CP-Ti (0.3 Fe, 0.35 O)	920
Grade 4	CP-Ti (0.5 Fe, 0.40 O)	950
Grade 7	Ti-0.2Pd	915
Grade 12	Ti-0.3Mo-0.8Ni	880
Ti 5-2.5	Ti-5Al-2.5Sn	1040
Ti 3-2.5	Ti-3Al-2.5V	935
<b>α + β Alloys</b>		
Ti-811	Ti-8Al-1V-1Mo	1040
IMI 685	Ti-6Al-5Zr-0.5Mo-0.25Si	1020
IMI 834	Ti-5.8Al-4Sn-3.5Zr-0.5Mo-0.7Nb	1045
Ti-6242	Ti-6Al-2Sn-4Zr-2Mo	995
Ti 6-4	Ti-6Al-4V (0.20 O)	995
Ti 6-4 ELI	Ti-6Al-4V (0.13 O)	975
Ti-662	Ti-6Al-6V-2Sn	945
IMI 550	Ti-4Al-2Sn-4Mo-0.5Si	975
<b>β Alloys</b>		
Ti-6246	Ti-6Al-2Sn-4Zr-6Mo	940
Ti-17	Ti-5Al-2Sn-2Zr-4Mo-4Cr	890
SP-700	Ti-4.5Al-3V-2Mo-2Fe	900
Beta-CEZ	Ti-5Al-2Sn-2Cr-4Mo-4Zr	890
Ti-10-2-3	Ti-10V-2Fe-3Al	800
Beta 21S	Ti-15Mo-2.7Nb-3Al-0.2Si	810
Ti-LCB	Ti-4.5Fe-6.8Mo-1.5Al	810
Ti-15-3	Ti-15V-3Cr-3Al-3Sn	760
Beta C	Ti-3Al-8V-6Cr-4Mo-4Zr	730
B120VCA	Ti-13V-11Cr-3Al	700

As the beneficial application of this class of titanium alloys has been recognized, their use significantly increased. Furthermore, specific alloys have been formulated to improve the environmental resistance of CP titanium and  $\alpha$  titanium alloys or to provide comparable performance at reduced cost where expensive additions such as palladium (Pd) are involved. Consequently, there has been an increase of alloy grades. Now, there are about 16 alloys or grades identified in sum. Table 2.2 lists these alloys and respective grade number belongs them, together with the composition limits of these alloys. The main difference between CP titanium grades is oxygen and iron content and oxygen content is the principal regulator of tensile properties. Grades of higher purity which means lower interstitial content are lower in strength and hardness, and have a lower transformation temperature, when compared to those higher in interstitial content [1, 9].



**Table 2.2:** Chemical composition and yield strength values for CP titanium and  $\alpha$  titanium alloys [1].

Grade or Alloy	O (max.)	Fe (max.)	Other Additions	$\sigma_{0.2}$ (MPa)
CP Titanium				
CP Titanium Grade 1	0.18	0.20		170
CP Titanium Grade 2	0.25	0.30		275
CP Titanium Grade 3	0.35	0.30		380
CP Titanium Grade 4	0.40	0.50		480
Ti-0.2Pd (Grade 7)	0.25	0.30	0.12-0.25Pd	275
Ti-0.2Pd (Grade 11)	0.18	0.20	0.12-0.25Pd	170
Ti-0.05Pd (Grade 16)	0.25	0.30	0.04-0.08Pd	275
Ti-0.05Pd (Grade 17)	0.18	0.20	0.04-0.08Pd	170
Ti-0.1Ru (Grade 26)	0.25	0.30	0.08-0.14Ru	275
Ti-0.1Ru (Grade 27)	0.18	0.20	0.08-0.14Ru	170
$\alpha$ Titanium Alloys				
Ti-0.3Mo-0.9Ni (Grade 12)	0.25	0.30	0.2-0.4Mo, 0.6-0.9Ni	345
Ti-3Al-2.5V (Grade 9)	0.15	0.25	2.5-3.5Al, 2.0-3.0V	485
Ti-3Al-2.5V-0.05Pd (Grade 18)	0.15	0.25	2.5-3.5Al, 2.0-3.0V (+Pd)	485
Ti-3Al-2.5V-0.1Ru (Grade 28)	0.15	0.25	2.5-3.5Al, 2.0-3.0V (+Ru)	485
Ti-5Al-2.5Sn (Grade 6)	0.20	0.50	4.0-6.0Al, 2.0-3.0Sn	795
Ti-5Al-2.5Sn ELI	0.15	0.25	4.75-5.75Al, 2.0- 3.0Sn	725
*For all grades, values for C and N are 0.08-0.10 and 0.03-0.05 respectively.				

All alloys in this class derive their characteristics from the hexagonal  $\alpha$  phase. For some purposes the class should be subdivided to allow a clearer discussion of behavior trends. All CP titanium grades are grouped together because none of the grades derive strength from the substitutional alloying elements (including Fe, Pd and Ru).

The major uses of CP titanium and other  $\alpha$  alloys are for process equipment in the chemical and petrochemical industries. This is the case if the applications are ranked by quantity of material used annually. There are a number of applications for CP titanium in other industrial sectors, including tube and shell heat exchangers, pressure vessels (commonly used because of strength, fabricability and corrosion resistance), emission control systems for coal burning power generation plants and bleaching section of the pulp and paper production equipment (due to highly corrosion resistance of CP titanium) [1, 9-10].

### 2.2 Titanium Alloys

Commercial titanium alloys are classified conventionally into three different categories ( $\alpha$  alloys,  $\alpha+\beta$  alloys, and  $\beta$  alloys) according to their position in a pseudo-binary section through a  $\beta$  isomorphous phase diagram, schematically shown in Figure 2.2. A list of the most important commercial alloys belonging to each of these three alloy groups were shown in Table 2.1. In this table the common name, the alloy composition, and the  $\beta$  phase transformation temperature were stated for each alloy group [1].

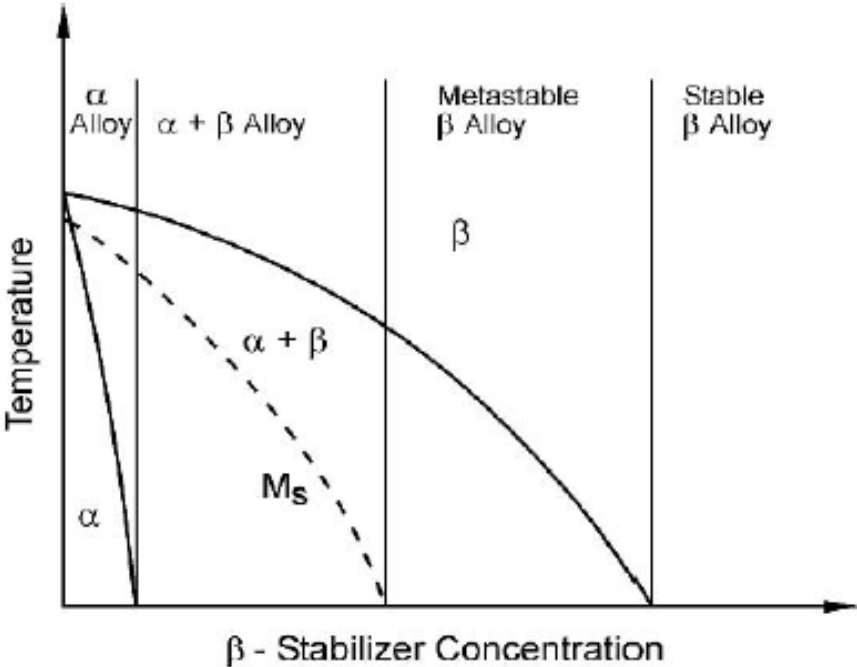


**Figure 2.2:** Pseudo-binary section through a  $\beta$  isomorphous phase diagram [1].

The group of  $\alpha$  alloys showed in Table 2.1 consist of the various grades of CP titanium and  $\alpha$  alloys, which upon annealing below the  $\beta$  transformation temperature contain; only small amounts of  $\beta$  phase (volumetrically 2-5%) stabilized by iron. CP titanium includes four different grades which are different from each other with respect to their oxygen content from 0.18% (Grade 1) to 0.40% (Grade 4), in order to increase the yield strength level of metal.

Classifying titanium alloys by their constitution ( $\alpha$  alloys,  $\alpha+\beta$  alloys and  $\beta$  alloys) can be eligible, but also become misleading. For example, essentially all  $\alpha$  alloys contain a small amount of  $\beta$  phase. All alloys in the group of  $\beta$  alloys are actually metastable  $\beta$  alloys, because they all are located in the equilibrium ( $\alpha+\beta$ ) phase region of the phase diagram.

Although the number of commonly used  $\beta$  titanium alloys in Table 2.1 are as large as the number of  $\alpha+\beta$  alloys, it should be kept in mind that, the percentage of  $\beta$  alloy usage on the total titanium market is very low. However, this percentage of  $\beta$  alloy usage is steadily increasing due to the attractive properties, especially the high yield strength level and for some applications (for example springs) the low modulus of elasticity [1].

### **2.3 Physical Properties**

For most application purposes, the preponderance of titanium's physical and chemical properties is much less important than its mechanical properties. Noteworthy exceptions are the low density and the formation of the protective oxide layer on the surface which has good corrosion resistance. Most of the properties of titanium are discussed in general terms, only a few of them are treated in some detail. These properties include diffusion, corrosion behavior and oxidation [11].

Being a low-density element (approximately 60% of the density of steel and super alloys), titanium can be strengthened greatly by alloying of some elements and processes like deformation and forging. In addition to the basic characteristics, some other selected properties of titanium are listed in Table 2.3 [9].

**Table 2.3:** Properties of titanium metal at room temperature [9].

Atomic number	22
Atomic Weight	47.90
Atomic Volume	10.6 W/D
Covalent Radius	1.32 Å
Ionization Potential	6.8282 V
Crystal Structure Alpha ( $\leq 882^{\circ}\text{C}$ ) Beta ( $\geq 882^{\circ}\text{C}$ )	Close-packed hexagonal Body-centered cubic
Color	Dark gray
Density	4.50 g/cm <sup>3</sup>
Melting Point	1668 °C
Solidus/Liquidus	1725 °C
Boiling Point	3260 °C
Specific Heat (at 25°C)	523 j/kg.K
Thermal Conductivity	14.99 W/m.K
Thermal Expansion Coefficient	8.36x10 <sup>-6</sup> K <sup>-1</sup>
Heat of Fusion	440 kJ/kg
Heat of Vaporization	9.83 MJ/kg
Hardness	≈ 70 HRB
Tensile Strength	240 MPa
Young's Modulus	120 GPa
Poisson's Ratio	0.361
Coefficient of Friction At 40 m/min At 300 m/min	0.8 0.68
Specific Gravity	4.5
Electrical Conductivity	3% IACS
Electrical Resistance	564.9x10 <sup>-9</sup> Ω.m

The property values for high-purity polycrystalline  $\alpha$  titanium (> 99.9%) at room temperature are not significantly different than those for the various CP titanium

grades. Thermal conductivity (14.99 W/m.K) is lower and electrical resistance ( $564.9 \times 10^{-9} \Omega \cdot m$ ) is higher for these commercial alloys, whereas the thermal expansion coefficient ( $8.36 \times 10^{-6} K^{-1}$ ) and the specific heat capacity (523 j/kg.K) are only slightly affected. The thermal conductivity and the electrical resistance both depend on the density and extent of scattering of the conductive electrons.

Comparing the values for titanium with other structural metallic materials like iron, nickel and aluminum, it can be seen that the thermal expansion coefficient is lower for titanium. Consequently, titanium alloys are an excellent choice for applications requiring high strength to density ratio and low thermal expansion; examples include casings for aero-engines and connecting rods in automobile engines [9].

## **2.4 Oxidation of Titanium**

Product of titanium's oxidation from the exposure to air is titanium dioxide ( $TiO_2$ ), which has a tetragonal rutile crystal structure. This oxide layer is often called scale and is an n-type anion-defective oxide, through which the oxygen ions can diffuse. The reaction front is at the metal/oxide interface and the scale grows into the titanium base material. The driving force for the rapid oxidation of titanium is the high chemical affinity of titanium to oxygen, which is higher than for nitrogen. During the oxidation process, the high affinity of titanium to oxygen and the high solid solubility of oxygen in titanium (about 14.5%) results in the simultaneous formation of the scale and an adjacent oxygen rich layer in the base metal. This oxygen rich layer is called  $\alpha$ -case because it is a continuous layer of oxygen stabilized  $\alpha$  phase. With this ability of passivation, titanium exhibits a high degree of immunity against attack by most mineral acids and chlorides [1, 9].

## **2.5 Crystal Structure**

Pure titanium exhibits an allotropic phase transformation at  $882^\circ C$ , changing from to a close packed hexagonal crystal structure ( $\alpha$  phase) at lower temperatures to a body centered cubic crystal structure ( $\beta$  phase) at higher temperatures. This allotropic phase transformation temperature is determined by interstitial and substitutional elements and therefore depends on the purity of the metal.

As shown in Figure 2.3, the hexagonal unit cell of  $\alpha$  phase is indicating the room temperature values of the lattice parameters  $a$  (0.295 nm) and  $c$  (0.468 nm). The resulting  $c/a$  ratio for pure  $\alpha$  titanium is 1.587, which is smaller than the ideal ratio of 1.633 for the hexagonal close-packed crystal structure. Lattice parameter value of pure  $\beta$  titanium at 900°C ( $a = 0.332$  nm). The close-packed directions are the four  $\langle 111 \rangle$  directions [1].

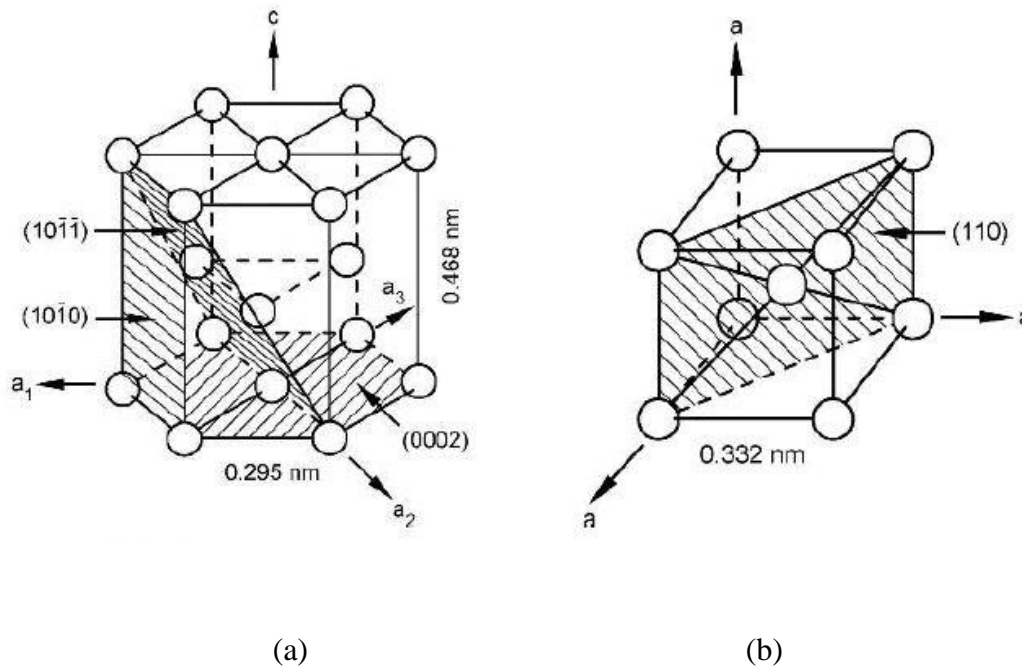


**Figure 2.3:** Unit cells of (a)  $\alpha$  and (b)  $\beta$  phases [1].

The transformation of the bcc  $\beta$  phase to the hexagonal  $\alpha$  phase in commercially pure titanium (CP titanium) and titanium alloys can occur martensitically or by a diffusion controlled nucleation and growth process depending on cooling rate and alloy composition.

Operation of alloying the titanium metal is dominated by the ability of elements to stabilize  $\alpha$  and  $\beta$  phases, and this behavior is related to the number of bonding electrons, the group number of the element concerned. Alloying elements with electron/atom ratios of less than 4 stabilize  $\alpha$  phase, elements with a ratio of 4 are neutral, and elements with ratios greater than 4 stabilize  $\beta$  phase [10].

### 3. NANOSTRUCTURED MATERIALS

Nanoscience is a multi disciplinary field that consists of applied physics, biology, materials science, chemical engineering, mechanical engineering, electronics and biotechnology and so on. There is a huge interest on this discipline and as a result, an exponential growth on nanoscience and nanotechnology research activities can be observed by the beginning of 21st century [12].

Today, nanostructured materials which refer to solids having nanoscale structures between 1 and 100 nm are available in a wide variety of shapes including symmetrical spheres and polyhedrons, cylindrical tubes and fibers, or random and regular pores in solids. In Figure 3.1, some examples from natural and artificial nano, micro and macrostructures, which are common in life. These materials in the following figure are distinctive from one to another and have different sizes with characteristic aspect ratios upon to several orders of magnitude [4].

The chain of single atoms shown at the bottom of Figure 3.1 can be considered as the tiniest possible nanostructure. Such nanostructures (e.g. phenylene–acetylene oligomers) have recently attracted attention as possible candidates for molecular wires for use in electronic applications. Short DNA oligomers are also prospective materials for tailoring molecular nanowires, due to their versatile chemistry which facilitates functionalization and the existence of technology for sequential DNA synthesis, allowing control over the structure of biomolecules [4].

The large class of elongated nanostructures with relatively small aspect ratios and a characteristic diameter in the range of sub to several nanometers, is represented by the elongated shape nanocrystals of semiconductor materials, which have evolved from the quantum dots so actively studied over the previous decade [4, 13].

In comparison to nanocrystals, single-walled carbon nanotubes (SWCN) have a much higher aspect ratio and a similar range of diameters, while multi-walled carbon nanotubes (MWCN), however, they are characterized by larger diameters and also very large aspect ratios.

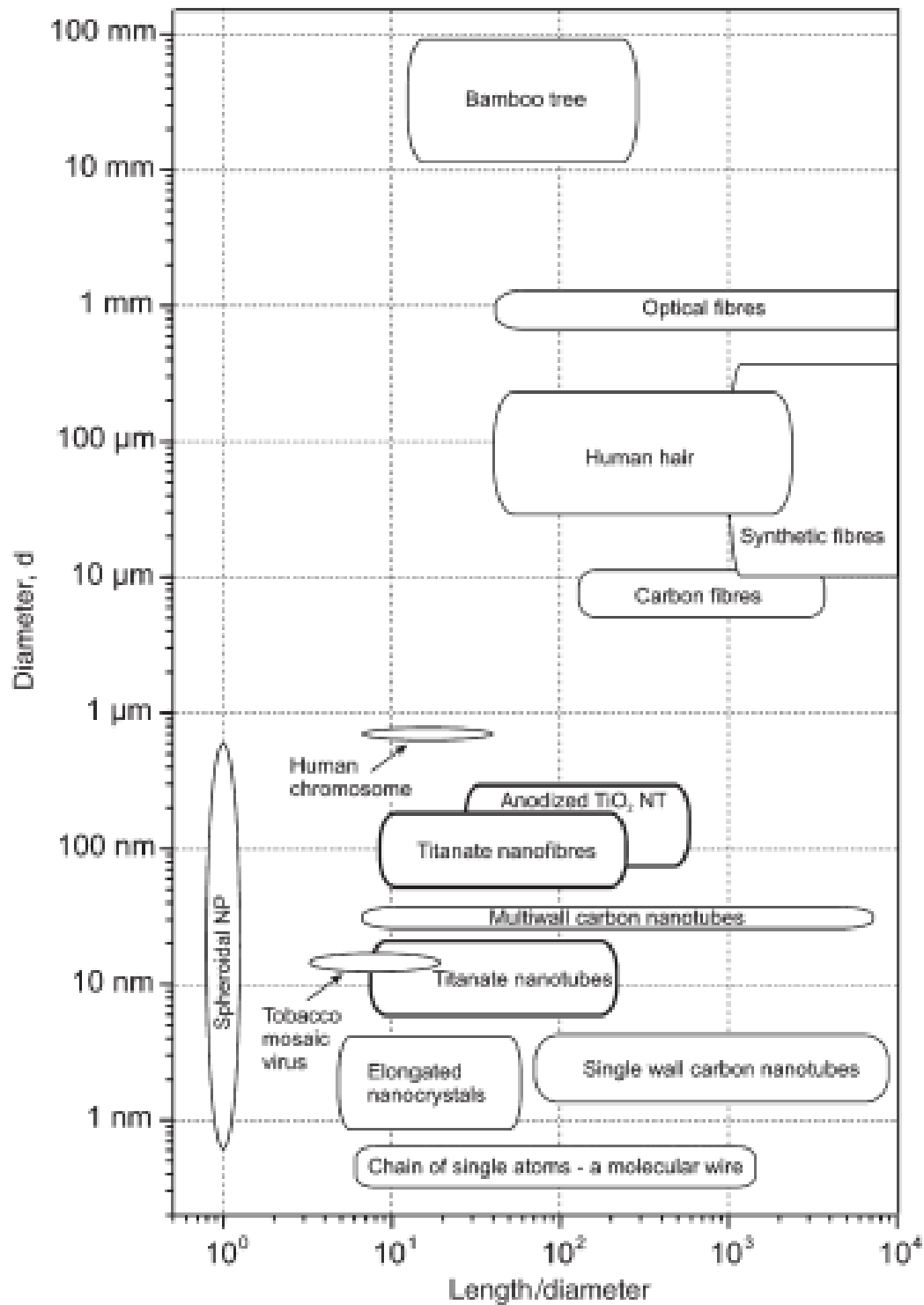


**Figure 3.1:** Structures with different sizes and aspects [4].

### 3.1 Nanotubes

Nanostructured materials have been with us for many centuries; however Carbon nanotubes are the milestone of nanomaterials studies, especially on nanotubes. In 1991, a paper by Sumio Iijima on carbon nanotubes stimulated recognition of the



importance and the structural elegance of these materials. Iijima's work on CNT's drew attention and catalyzed an interest in this topic, with lots of scientific papers on nanomaterials being published from the beginning of 1990's [4].

After the discovery of carbon nanotube (CNT), large attention has been paid to this unique low-dimensional nanostructured materials because of its attractive various physical and chemical functions which arise from the synergy of low-dimensional nanostructure and anisotropy of carbon network, thus known as graphene structure. Until now, not only large numbers of fundamental studies on the structural, electrical, optical, mechanical, and physicochemical properties but also application-oriented research and development, such as single-electron transistor device, field emission device, fuel cells, and strengthening fillers of composites, have been extensively carried out. Alongside CNTs, various inorganic nanotubular materials have been reported in non-oxide compounds, boron nitride (BN) and molybdenum disulfide ( $\text{MoSi}_2$ ); in oxides such as vanadium oxide ( $\text{V}_2\text{O}_5$ ), aluminum oxide ( $\text{Al}_2\text{O}_3$ ), silicon dioxide ( $\text{SiO}_2$ ) and titanium oxide ( $\text{TiO}_2$ ) and also in natural minerals like imogolite [13].

In this chapter, main nanotube structures; carbon nanotubes, metal chalcogenide nanotubes and metal oxide nanotubes will be discussed because of their importance in nanotubes field and relevance to this thesis work.

### **3.1.1 Carbon nanotubes**

Carbon nanotubes (CNTs), known as the turning points of nanostructured materials; especially the nanotubes, were discovered in 1991 as a minor by product of fullerene synthesis [14]. An observable progress has been made in the following years of discovery, including the discovery of two fundamental nanotube types, these are single-wall (SWNT) and multi-wall (MWNT). There have been very important steps taken in carbon nanotubes' synthesis and purification, clarification of the fundamental physical properties, and important strides are being taken toward realistic practical applications [15]. Just like having lots of different properties, CNTs also have alternative production methods and these methods can be counted mainly as arc-evaporation, high temperature heat treatments, laser vaporization, catalytic chemical vapor deposition and electrochemical synthesis techniques [16].

The wide range of fascinating properties of carbon nanotubes provides attractive opportunities for technological applications. Some are realistic and likely to be commercial in the future, while others are in the development stage. These applications include field effect transistors, electron sources for field emissions, supercapacitors, actuators, sensors, probes, lithium batteries and hydrogen storage.

Carbon nanotubes are long cylinders of 3-coordinated carbon, slightly pyramidalized by curvature from the pure  $sp^2$  hybridization of graphene, toward the diamond-like  $sp^3$  [17]. Infinitely long in principle, a perfect tube is capped at both ends by hemi-fullerenes, leaving no dangling bonds. A single-wall carbon nanotube is one such cylinder, while multi-wall tubes consist of many nested cylinders whose successive radius differ by roughly the interlayer spacing of graphite as seen in Figure 3.2 [15].

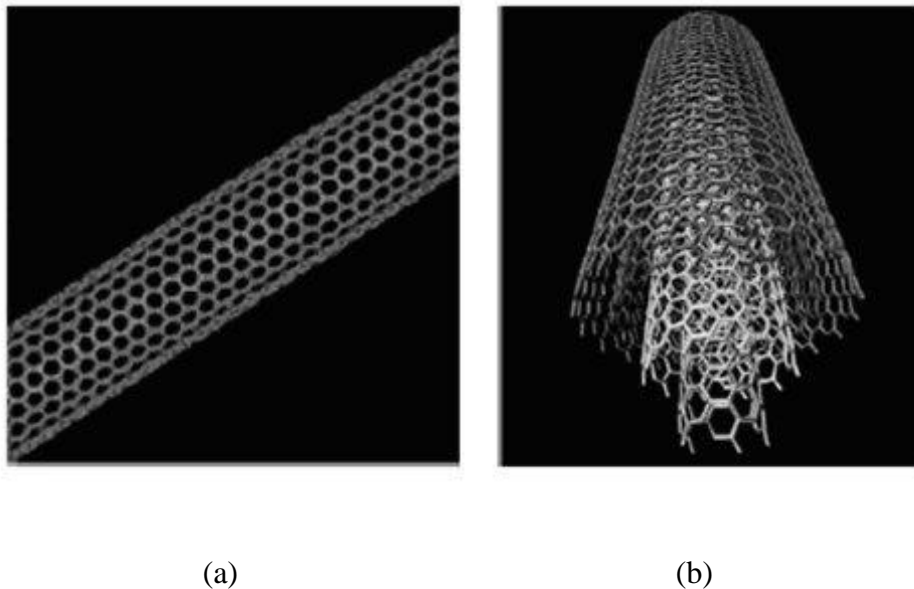


**Figure 3.2:** Images of (a) SWNT and (b) MWNT [15].

Strength of the carbon–carbon bond makes an increase to the interest in the mechanical properties of carbon nanotubes. Theoretically, carbon nanotubes should be stiffer and stronger than any other substance ever known. Simulations and experiments demonstrate a remarkable “*bend, do not break*” response of individual SWNT to large transverse deformations; an example from Yakobson’s simulation is shown in Figure 3.3 [18]. The prove of this mechanical superiority of carbon nanotubes is mainly about their Young’s modulus; Young’s modulus of a cantilevered individual MWNT can be up to 1.8 TPa, the amplitude of thermally driven vibrations observed in the TEM [19].

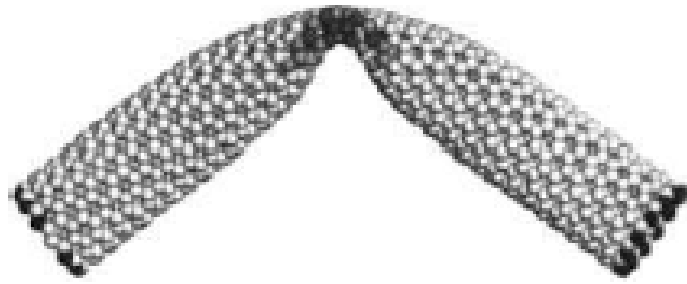


**Figure 3.3:** Simulation of a large-amplitude transverse deformation of a carbon nanotube [18].

When the computer-generated elastic limit beyond force removed, the tube snaps back. Since, there is no plastic deformation on CNTs are observed.

Just like their physical properties, CNTs exhibit good chemical properties. They are highly resistant to chemical attack; it is difficult to oxidize them and the onset of oxidation in nanotubes is 100°C higher than that of carbon fibers. As a result, temperature is not a limitation in practical applications of nanotubes.

### **3.1.2 Metal chalcogenide nanotubes**

Chalcogenides of transition metals having multi-walled nanotubular morphology have been intensively studied from the discovery of CNTs. The methods of metal chalcogenide nanotube preparation include arc discharge, laser ablation, sublimation, gas phase reduction with H<sub>2</sub>S or H<sub>2</sub>Se, pyrolysis of (NH<sub>4</sub>)<sub>2</sub>MX<sub>4</sub> (where M=Mo or W; X=S or Se) and hydrothermal reactions [4]. A summary of these inorganic nanotubes and their production method is indicated in the Table 3.1 with comments [15].

**Table 3.1:** Summary of the inorganic nanotubes reported in literature and the synthetic procedures used for their production [15].

Compound	Synthetic Approach	Comment
MS <sub>2</sub> (M=W, Mo)	Reaction with the respective oxide at elevated temperature Chemical Vapor Transport (CVT)	
ReS <sub>2</sub>		ReS <sub>2</sub> is a 2D compound with Re-Re bonds
Single wall MoS <sub>2</sub> nanotubes	CVT(I <sub>2</sub> ) + C <sub>60</sub> catalyst	
MoS <sub>2</sub>	Ammonium thiometallate solution in porous alumina template Heating MoS <sub>2</sub> powder in a closed Mo crucible Hydrothermal reaction of ATM Firing of ATM in H <sub>2</sub> Firing of MoO <sub>3</sub> nanobelts in the presence of sulfur Microwave plasma	Not perfectly crystalline
NbS <sub>2</sub> , ReS <sub>2</sub>	Depositing NbCl <sub>2</sub> (ReCl <sub>3</sub> ) from solution onto carbon nanotubes	
NbSe <sub>2</sub>	Direct reaction of elements at 800°C	
WS <sub>2</sub>	Firing of ATM in thiophene/hydrogen at 360 – 450°C Hydrothermal synthesis with organic amines and a cationic surfactant Growth of WO <sub>3</sub> nanowhiskers	
TiS <sub>2</sub>	CVT(I <sub>2</sub> )	
InS	Reacting t-Bu <sub>3</sub> In with H <sub>2</sub> S in aprotic solvent at 203°C in benzenethiol	Metastable phase

### 3.1.3 Metal oxide nanotubes

Metal oxide nanotubes mainly emerged from the invention of aluminum oxide nanotubes, which is produced via anodic oxidation in acidic electrolytes and discovered in pre-nanoscience era [20]. Just like aluminum oxide nanotubes, many kinds of oxide nanotubes fabricated via either anodization method or hydrothermal synthesis techniques such as Barium titanate nanotubes, Hafnium oxide nanotubes, Cobalt oxide nanotubes, Iron oxide nanotubes, Magnesium hydroxide nanotubes, Lead titanate nanotubes and most importantly Titanium dioxide nanotubes. There are some examples of metal oxide nanotubes produced with different methods;  $\text{MnO}_2$ ,  $\text{VO}_x$ ,  $\text{ZrO}_2$ ,  $\text{Ni}_3\text{Si}_2\text{O}_5(\text{OH})_4$  and  $\text{Mg}_3\text{Si}_2\text{O}_5(\text{OH})_4$  nanotubes alongside with a metal chalcogenide nanotube  $\text{WS}_2$  in Figure 3.4 [4].

In conclusion to this variety of such different metal oxide or metal chalcogenide nanotubes, elongated inorganic nanostructures are constantly growing because of the interest in new nanomaterials with various morphologies. Due to the lack of a general theory regarding nanostructure growth (nanotubes, nanofibers and nanorods) which could allow for the prediction of the synthesis conditions required for new nanomaterials, current works apply the trial and error methods [21].

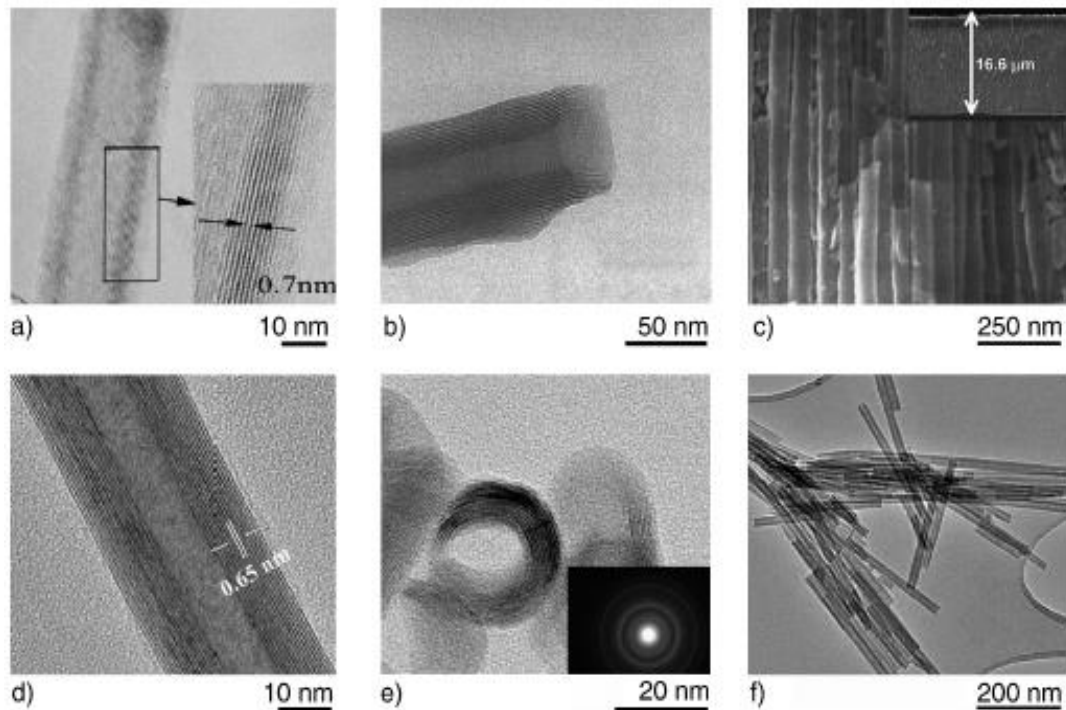


**Figure 3.4:** SEM images of (a)  $\text{MnO}_2$ , (b)  $\text{VO}_x$ , (c)  $\text{ZrO}_2$ , (d)  $\text{WS}_2$ , (e)  $\text{Ni}_3\text{Si}_2\text{O}_5(\text{OH})_4$  and (f)  $\text{Mg}_3\text{Si}_2\text{O}_5(\text{OH})_4$  nanotubes [4].



## 4. TITANIUM DIOXIDE NANOTUBES

Amongst nanomaterials; especially nanotubes, TiO<sub>2</sub> nanotubes are one of the most encouraging nanostructured oxides with tubular structure because of their both macro and microscale applications. TiO<sub>2</sub> is well known as a wide gap semiconductor oxide (3 eV for rutile and 3.2 eV for anatase). However, it is inexpensive, chemically stable, environmentally friendly and has no absorption in the visible light region; instead of it, it only absorbs UV light (down to 400 nm); electron and hole pair is generated by the UV irradiation, inducing chemical reactions at the surface. Therefore, the most promising characteristic of TiO<sub>2</sub> lies in its photochemical properties such as high photocatalytic activity. Due to this reason, titania nanotubes have been the subjects of studies from 1950s to utilize TiO<sub>2</sub> as a photocatalyst, an electrode of dye-sensitized solar cell, a gas sensor, and so on [12, 13].

### 4.1 Synthesis Techniques

For TiO<sub>2</sub> nanostructured materials, two main synthesis techniques can be count: templated and non-templated procedures, as illustrated in Figure 4.1 [20]. When it is about the elongated structures like nanotubes and nanowires, two common non-templated methods are valid. These are alkaline hydrothermal synthesis and electrochemical anodizing of CP titanium.

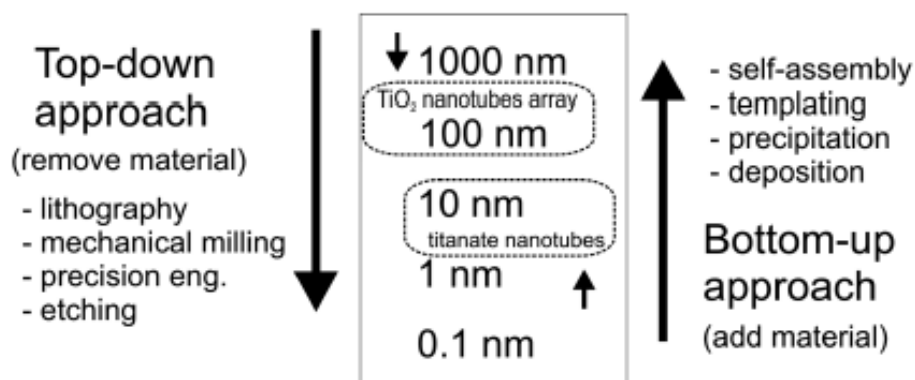


**Figure 4.1:** Top-down and bottom-up approaches for TiO<sub>2</sub> nanomaterials [20].

### 4.1.1 Template methods

The method of template synthesis of nanostructured materials, being a classical “*bottom-up*” method, that utilizes the morphological properties of known and characterized materials in order to construct materials having a similar morphology by methods including reactive deposition. Template method is very general; adjusting the morphology of template material is enough to prepare numerous materials having the desired properties. A disadvantage is that, the template material is sacrificial and needs to be destroyed after synthesis leading to increased cost of materials in most cases. As in the case of all surface finishing techniques, it is also important to maintain a high level of surface cleanliness to ensure good adhesion between the substrate and the surface coating.

Template method consists of a few steps, also shown in Figure 4.2 [20]. The first step is the deposition of required materials onto the surface and into the pores of the templated substrate via some deposition techniques, such as sol-gel deposition, atomic layer deposition (ALD) and chemical vapor deposition (CVD). After adhesion of material, the template is removed by some methods which are including pyrolysis, selective etching and dissolution.

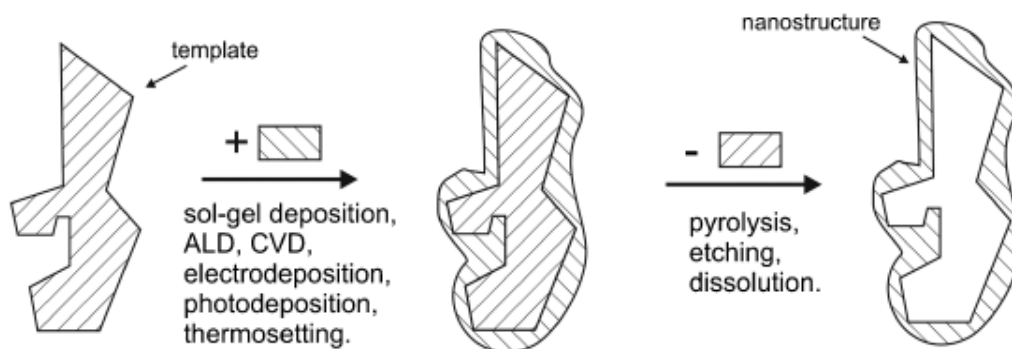


**Figure 4.2:** Template method for the preparation of nanostructured materials [20].

### 4.1.2 Alkaline hydrothermal synthesis of elongated titanates

It is possible to consider titanium dioxide as an amphoteric oxide, as a result of its capability to interact reaction with either strong acid forming titanium (IV) salts (e.g. titanium (IV) chloride,  $\text{TiCl}_4$ ; or titanil sulfate,  $\text{TiOSO}_4$ ), or with strong bases forming titanate salts with the general formula  $\text{M}_{2n}\text{Ti}_m\text{O}_{2m+n}\cdot x\text{H}_2\text{O}$  (where M is an alkaline metal cation and n, m and x are integers; e.g.  $\text{Na}_2\text{Ti}_6\text{O}_{13}$ ). Although the solubility of  $\text{TiO}_2$  in strong acid might be relatively high, it is usually much lower in



most of basic solutions; nevertheless, the solubility of  $\text{TiO}_2$  can be increased by increasing the temperature of solution in many cases.

Traditionally, titanates are produced by either solid state or melt reaction between  $\text{TiO}_2$  and a second metal oxide or carbonate at elevated temperatures ( $> 1000^\circ\text{C}$ ), to form bulk titanate crystals. On the contrary, the alkaline hydrothermal treatment of  $\text{TiO}_2$  at elevated temperatures and pressure can provide an alternative route for the synthesis of nanostructured titanates, via a sequence involving the dissolution of the initial  $\text{TiO}_2$  and the crystallization of the final product.

There are a few examples of titanate nanotubes and nanofibers produced by alkaline hydrothermal techniques as seen on Figure 4.3 [19].

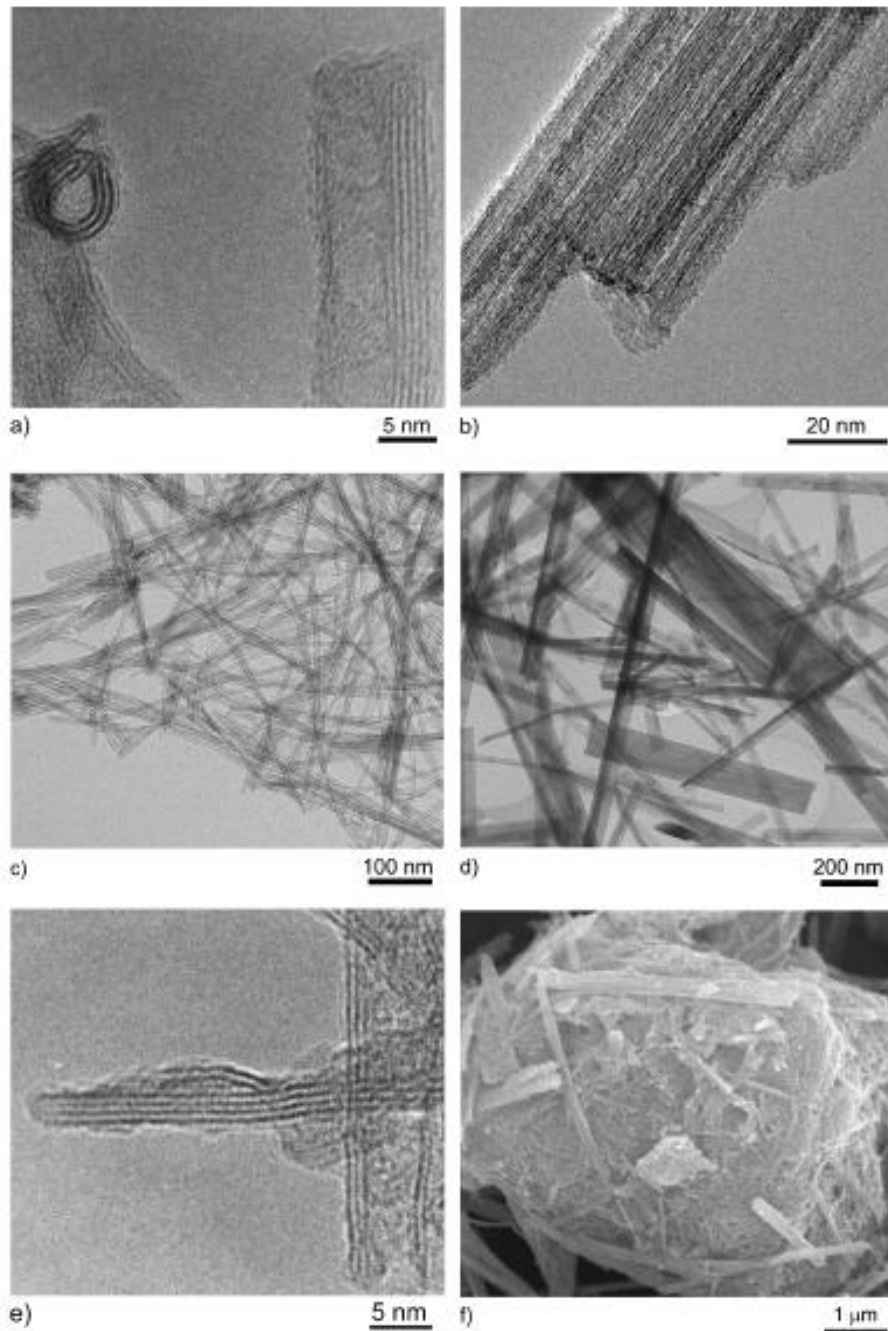


**Figure 4.3:** TEM images of (a) and (c) titanate nanotubes, (b) and (d) nanofibres, (e) multilayer nanosheets and a SEM image of (f) an agglomerate of titanate nanotubes produced by alkaline hydrothermal treatments [19].

#### 4.1.3 Anodic oxidation

Recent researches in the area of anodization of titanium metal were focused on the preparation of the non-porous and corrosion-resistant film of  $\text{TiO}_2$ . However, technological improvements in nanotechnology and the demand for new nanomaterials have stimulated the development of methods for preparing porous  $\text{TiO}_2$  films. It is known that, the addition of fluoride ions to an aqueous electrolyte

solution can significantly lower the corrosion resistance of titanium and TiO<sub>2</sub> coatings, due to the formation of pitting channels. Based on this effect, a new method to produce nanoporous TiO<sub>2</sub> films has been established using fluoride-containing electrolytes. There are some SEM images of TiO<sub>2</sub> nanotube arrays can be seen in Figure 4.4 [22].

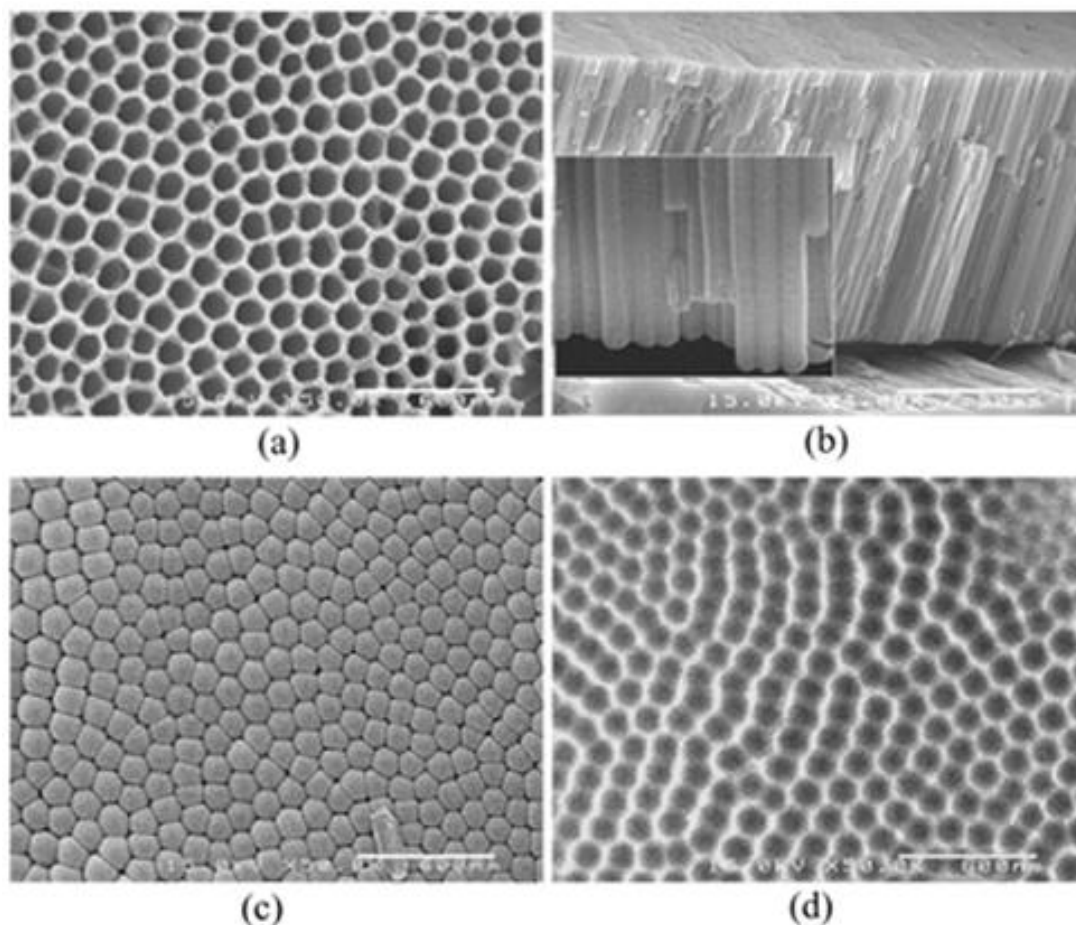


**Figure 4.4:** Typical SEM images of TiO<sub>2</sub> nanotube arrays [22].

## 4.2 Applications of Titanium Dioxide Nanotubes

Characteristic features such as elongated morphology, high specific surface area and wettability properties, provide TiO<sub>2</sub> nanostructures to be used in many applications. These applications include hydrogen storing, photoelectrochemical water splitting and energy conversion.

It is known that titanium has an affinity for absorbing hydrogen. In CP titanium and  $\alpha$  alloys, this affinity is manifested as a relatively low solubility and the accompanying formation of the titanium hydride phase which is TiH<sub>2</sub>. This situation

makes CP titanium and  $\alpha$  alloys unsuitable for hydrogen storage by reason of, it limits the amount of hydrogen per unit volume that can be stored in titanium. Nevertheless, titanium based hydrogen storage systems remain attractive because of their lightweight and thermodynamic feasibility of using titanium as a storage. Consequently, studies to develop hydrogen storing devices mainly focused on intermetallic compounds; such as TiFe and TiMn until the discovery of hydrogen storage properties of titanium dioxide nanotubes [4, 9].

Like hydrogen storing applications, anodized TiO<sub>2</sub> nanotube arrays have become the subject and been studied as a promising electrode for the photoelectrolysis of water. A photoelectrochemical system combines the harvesting of solar energy with electrolysis of water. When a semiconductor of proper characteristics is immersed in an aqueous electrolyte and irradiated with sunlight, sufficient energy is generated to split water into hydrogen and oxygen. Although the TiO<sub>2</sub> nanotube array architecture possesses high surface to volume ratios and large internal surface areas to be in contact with the electrolyte, TiO<sub>2</sub>'s responsive to UV light is only a small fraction (4%) of the sun's energy; while visible light comprises approximately 45%. For this reason, to use TiO<sub>2</sub> nanotube arrays in photocatalysis applications some treatments are applied such as heat treatment to increase the defects in structure while having a crystalline structure and adding doppants to modify the band gap of material [23].

Photocatalytic processes during the oxidation of organics in titanium dioxide nanotubes are illustrated in Figure 4.5 [4].

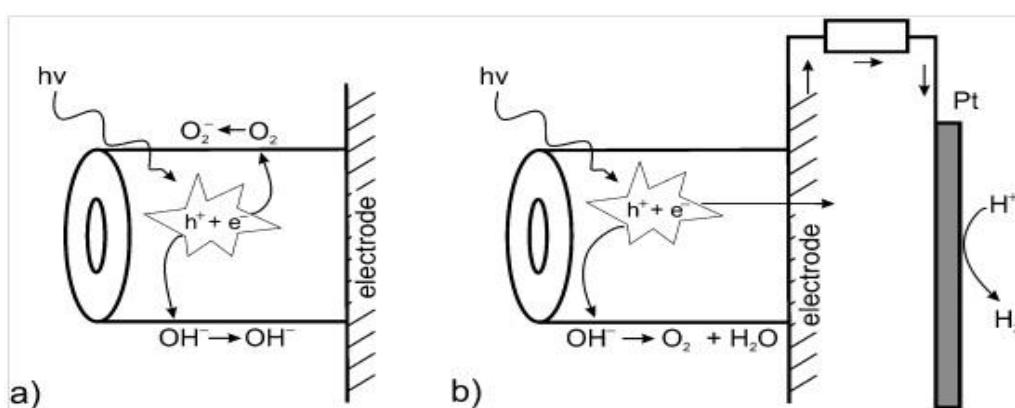


**Figure 4.5:** Photocatalytic processes: (a) initial photocatalytic reactions and (b) the process of photochemical water splitting on TiO<sub>2</sub> nanotubes [4].

## 5. THE ELECTROCHEMICAL ANODIZATION PROCESS

Anodization is an electrolytic process that creates a protective or decorative oxide film over a metallic surface. Anodization typically increases both the thickness and density of the oxide layer that forms on any metal surface exposed to the earth's atmosphere. To accomplish this oxide layer, the conducting piece undergoing anodization is connected to the positive terminal of a DC power supply and placed in an electrolytic bath where it serves as the anode. Generally, the cathode is a plate or rod of platinum because of platinum's superior electrical properties and resistance to acidic solutions; however materials like stainless steel can also be used. When DC power is applied to system, electrons are forced from the electrolyte to the anode and the process leaves surface metal atoms exposed to oxygen ions within the electrolyte bath. The atoms react and become an in situ integral part of the oxide layer. An illustration of an electrochemical anodization cell is shown in Figure 5.1 [23].

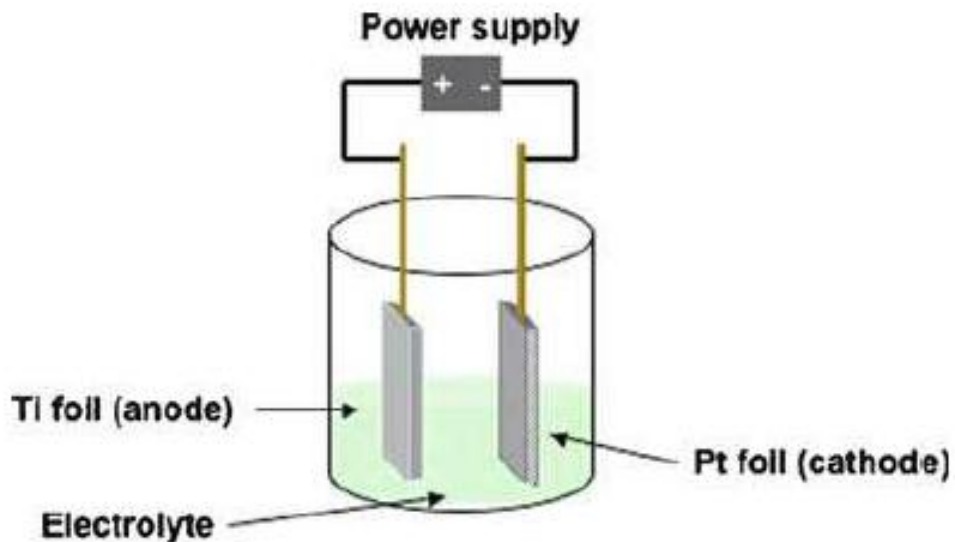


**Figure 5.1:** Schematic view of an electrochemical cell in which titanium samples (anode) are anodized with the help of platinum cathode [23].

The electrolyte composition is also the primary determinant of whether the oxide film is porous or if it forms a barrier layer. Oxide barrier layers grow in those neutral or slightly alkaline solutions in which titanium dioxide is largely insoluble. Porous

oxide layers grow in acidic electrolytes with fluoride or chloride ions in which oxide forms and then rapidly dissolve; also the acid cations affect the resulting nanotube array structures.

### 5.1 Effect of Cathode Materials

In metals anodization, both anode and cathode distinctively have an effect on reaction rates and overvoltage. As a result, overvoltage is the excess potential required for the discharge of an ion at an electrode over and above the equilibrium potential of the electrode. Consequently, overvoltage does play a very important role in the manner of morphology, dimensions as well as growth rate of the nanotubes, based on the dissolution kinetics of the titanium anode and in turn, the activity of the electrolyte bath and morphology of the architectures.

Platinum is commonly used as the cathode material for anodization processes due to its high catalytic activity and hence low overpotential losses in addition to its high stability. However, platinum is not the only option for any anodization operations, there are also some other materials available for cathode selection. Cathode metals can be mainly divided into three groups as listed in Table 5.1. These cathode metals are available to be used in both aqueous electrolytes and ethylene glycol electrolytes [24].

**Table 5.1:** Cathode materials used in TiO<sub>2</sub> anodization [24].

Pt Group Elements	Ni
	Pd
	Pt
Non-Pt Transition Elements	Fe
	Co
	Cu
	Ta
	W
Non-Transition Elements	C
	Al
	Sn

Results compiled from literature confirm that the nature of the cathode material plays a critical role in determining of surface appearance. The overpotential of the cathode is a critical factor that affects the dissolution kinetics of the titanium anode and in turn, the activity of the electrolyte and morphology of the architectures in TiO<sub>2</sub> nanotube production processes.

## **5.2 Anodic Oxidation of Titanium**

With a titanium anode and a selected cathode (e.g. platinum, stainless steel etc.) immersed in an aqueous electrolyte of dilute acid to which a small DC voltage is applied, the surface layer is sufficiently resistive to prevent current flow. Increasing the applied voltage produces no additional current flow until a threshold level is reached where the electric field intensity within the barrier is sufficient to force oxygen ions to diffuse across it, producing an ionic current. These oxygen ions react with the metal and increase the thickness and/or density of the oxide barrier. This process of high-field ionic conduction is central to anodization. Surely, the same process liberates hydrogen gas from the cathode. Since the electrical resistance of the layer increases in proportion to its thickness and since the rate of oxide growth is proportional to the current density, the thinner portions of the layer carry more current than the thicker ones. Hence, a thin section grows faster than a thick one, creating an even more uniform layer. As the layer thickens, the applied voltage required in order to maintain constant current does increase. The process continues until, for a given bath composition and temperature, a maximum applied voltage is reached above which other, non-desired reactions like oxygen evolution and solute oxidation become manifest. The dissolution of titania nanotube at higher voltage indicates field-assistant chemical dissolution of the oxide at the oxide–electrolyte interface. Due to the applied electric field, the Ti–O bond undergoes polarization and is weakened, promoting dissolution of the metal oxide. Increasing the anodizing time has little effect on the inner diameters of the nanotubes [25].

Fabrication of TiO<sub>2</sub> nanotube arrays via anodic oxidation of Titanium was first reported in 2001 by Gong and co-workers [3]. Later studies focused on precise control and extension of the nanotube morphology, length and pore size and wall thickness.

### 5.2.1 Mechanism of nanotube growth

It is possible to consider that, the main steps responsible for anodic formation of nanoporous alumina [26] and TiO<sub>2</sub> [27, 28] seem to be the same and they are fundamental to the formation of TiO<sub>2</sub> nanotube arrays. These steps are:

1. Oxide growth at the metal surface due to interaction of the metal with O<sup>2-</sup> or OH<sup>-</sup> ions. After an initial oxide layer formation, these anions migrate through the oxide layer reaching the metal/oxide interface where they react with the metal [26].
2. Ion (Ti<sup>4+</sup>) migration from the titanium at the metal/oxide interface; Ti<sup>4+</sup> cations will be ejected from the metal/oxide interface under application of an electric field that moves toward the oxide/electrolyte interface.
3. Field-assisted dissolution of the oxide at oxide/electrolyte interface [26, 29]. Due to the applied electric field, the Ti–O bonds undergo a polarization and these bonds are weakened by promoting dissolution of the cations. Ti<sup>4+</sup> cations dissolve into the electrolyte and the free O<sup>2-</sup> anions migrate to the metal/oxide interface, process (1) to interact with the titanium [30, 31].
4. Finally, chemical dissolution of the titanium or oxide, by the acidic electrolyte; chemical dissolution of TiO<sub>2</sub> in the HF electrolyte plays a key role in the formation of nanotubes rather than simple nanoporous structures.

For better control over the morphology and the degree of ordering in nanotubes, it is important to understand the underlying principles and mechanism for the formation of aligned nanotubes under anodic conditions. The growth of nanotubes by anodizing titanium can be described as a selective etching and the method can be related to a “*top down*” approach. With the most basic approaching, such nanotube growth can be described in terms of a competition between several electrochemical and chemical reactions.

In aqueous electrolytes and at a constant potential, most valve metals give rise to current–time curves with an exponential decay shape, due to the passivation of the electrode surface as a result of the formation of a barrier layer of low conductivity metal oxide. In contrast, the addition of HF or another source of fluoride ions, may result in an initial exponential decrease of current (phase a) followed by an increase



(phase b) to the quasi steady-state level (phase c). The steady-state level and the rate of the current recovery are increased with an increase in fluoride concentration.

Typically, such behavior of the current can be ascribed to different stages in the pore formation process, as schematically illustrated in Figure 5.2 (where drawings a, b and c correspond to the phases a, b and c in the current–time curve for fluoride-containing electrolyte) [4].

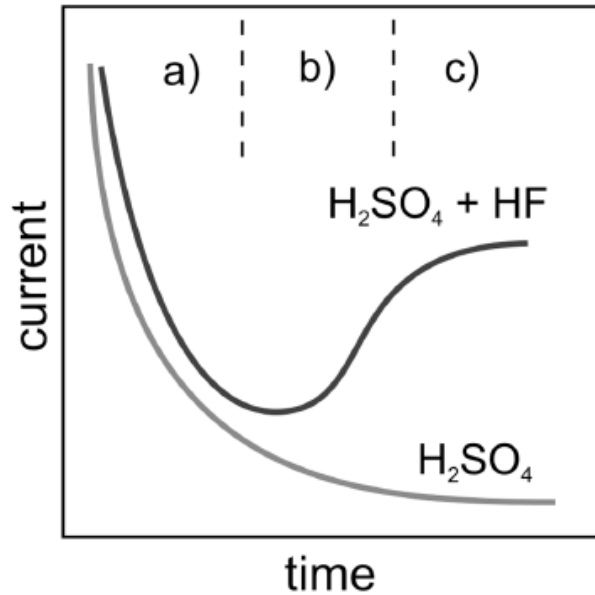


**Figure 5.2:** Current – Time curve. (a) oxide barrier formation, (b) pores start to grow, (c) steady state of nanotube growth [4].

As the anodization starts, the initial oxide layer [31] formed due to interaction of the surface  $Ti^{4+}$  ions with  $O^{2-}$  ions in the electrolyte, can be seen to uniformly spread across the surface. At the anode, oxidation of the metal releases  $Ti^{4+}$  ions and electrons, as shown in Equations 5.1, 5.2 and 5.3[32]:



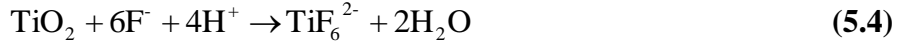
Hydrogen evolution occurs at the cathode:



The overall process of oxide formation is given by:



Fluorine ions can attack the oxide and hydrated layer; or the ions being mobile in the anodic layer under the applied electric field, react with  $\text{Ti}^{4+}$  as shown in Equations 5.4, 5.5 and 5.6 [33]:



During the initial stages of the anodization process, field-assisted dissolution dominates chemical dissolution due to the relatively large electric field across the thin oxide layer [34]. Small pits formed due to the localized dissolution of the oxide, act as pore forming centers, after which these pits convert into pores with increasing pore density, uniformly, over the surface. The pore growth occurs due to the inward movement of the oxide layer at the pore bottom (barrier layer). The  $\text{Ti}^{4+}$  ions migrating from the metal to the oxide/electrolyte interface dissolve in the HF electrolyte [31]. The rate of oxide growth at the metal/oxide interface and the rate of oxide dissolution at the pore-bottom/electrolyte interface ultimately become equal; thereafter the thickness of the barrier layer remains unchanged although it moves further into the metal increasing the pore depth. The thickness of the tubular structure ceases to increase when the chemical dissolution rate of the oxide at the mouth of the tube (nanotube array surface) becomes equal to the rate of inward movement of the metal/oxide boundary at the base of the tube. Higher anodization voltages increase the oxidation and field assisted dissolution and hence, a greater nanotube layer thickness can be achieved before equilibrating with chemical dissolution.

With anodization onset a thin layer of oxide forms on the titanium surface (Figure 5.3a). Small pits originate in this oxide layer due to the localized dissolution of the oxide (Figure 5.3b) making the barrier layer at the bottom of the pits relatively thin which, in turn, increases the electric field intensity across the remaining barrier layer resulting in further pore growth (Figure 5.3c). The pore entrance is not affected by electric field assisted dissolution and hence remains relatively narrow, while the electric field distribution in the curved bottom surface of the pore causes pore

widening, as well as deepening of the pore. The result is a pore with a scallop shape [35, 36]. These nanotube formation steps are illustrated in Figure 5.3 [37].

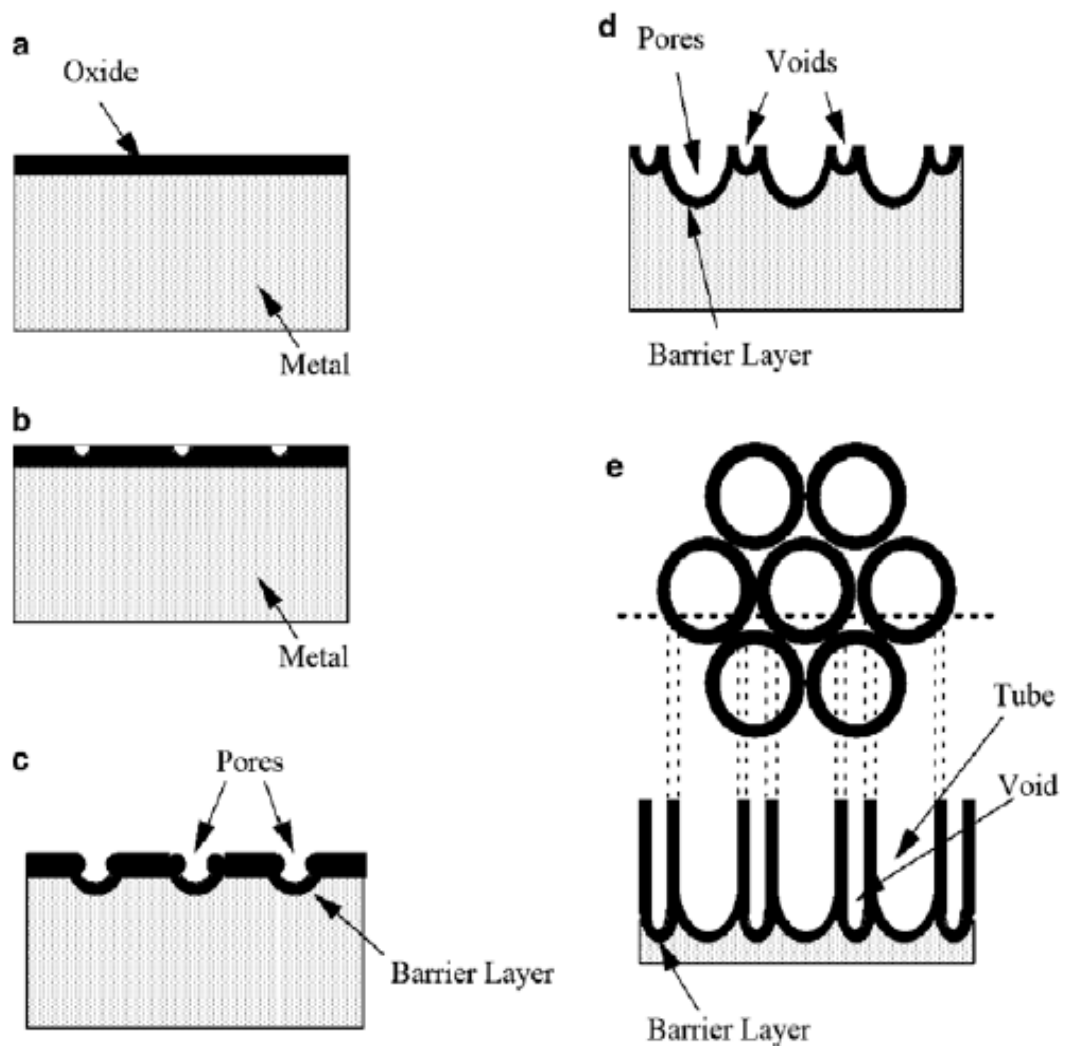


**Figure 5.3:** Illustration of nanotube formation at constant anodization voltage. (a) Oxide layer formation, (b) pit formation, (c) growth of pits into pores, (d) oxidation and field assisted dissolution, (e) nanotubes [37].

As the Ti–O bond energy is high (323 kJ/mol), in the case of TiO<sub>2</sub> it is reasonable to assume that only pores having thin walls can be formed due to the relatively low ion mobility and relatively high chemical solubility of the oxide in the electrolyte, hence un-anodized metallic portions can initially exist between the pores. As the pores grow deeper, the electric field in these protruded metallic regions increases; which enhances field assisted oxide growth and oxide dissolution. Consequently, simultaneously with the pores well-defined inter-pore voids start forming as shown in Figure 5.3d. Thereafter, both voids and tubes grow in equilibrium. The nanotube length increases until the electrochemical etch rate equals the chemical dissolution

rate of the nanotube top surface. After this point is reached, the nanotube length will be independent of the anodization time, as determined for a given electrolyte concentration and anodization potential.

Chemical dissolution, the key for self-organized formation of the nanotube arrays, reduces the thickness of the oxide layer (barrier layer) keeping the electrochemical etching (field assisted oxidation and dissolution) process active. If the chemical dissolution is too high or too low, no nanotubes can be formed. The electrochemical etch rate depends upon anodization potential as well as electrolyte concentrations. If the electrochemical etch proceeds faster than chemical dissolution the thickness of the barrier layer increases, which in turn reduces the electrochemical etching process to the rate determined by chemical dissolution. The chemical dissolution rate is determined by the  $F^-$  concentration and solution pH. With increasing  $F^-$  and  $H^+$  concentrations chemical dissolution increases. Investigations have indicated that for aqueous electrolytes, only in a fixed  $F^-$  concentration range can nanotube arrays be achieved. The anodic potential, at which nanotubes are formed, is related to the  $F^-$  ion concentration, with higher potentials requiring electrolytes of higher  $F^-$  concentration. If the titanium oxide either in the wall or at the pore bottom dissolves at a balance rate, the pore depth keeps constant and does not change with anodizing time. Moreover, breakdown sometimes occurs again inside the repassivated pores; it looks like there is the formation of small pores inside the existing pores. This kind of structure often takes place when increasing anodizing time and using strong acids like  $HNO_3$  as well as HF acid. This can be explained as; longer anodizing time and stronger acid facilitate crystallization and breakdown of titania nanotubes [25].

About the morphology of nanotubes, there are four main points to be indicated. These are nanotube diameter, nanotube length, ordering of nanotube arrays and lastly wall thickness of nanotubes. These morphological parameters strongly depend on electrolyte properties, electrode potential and anodization time. Literature reviews show that, increasing electrolyte potential and anodization time may cause increase in nanotube diameter and nanotube length but nothing is certain yet. Like nanotube diameter and length, ordering of nanotube arrays is also related to electrode potential. Acidic concentration of electrolyte slightly reduces the wall thickness of nanotubes, however this explanation is only valid for fluoride containing electrolytes as there is no much research on this subject [4].

## 6. EXPERIMENTAL STUDIES

The experimental sections of this thesis work mainly consist of following steps; preparation of CP titanium samples, anodic oxidation of prepared samples, annealing of anodized samples and lastly characterization studies. Treatments applied to CP titanium sample from polishing to annealing stages are schematized in Figure 6.1.

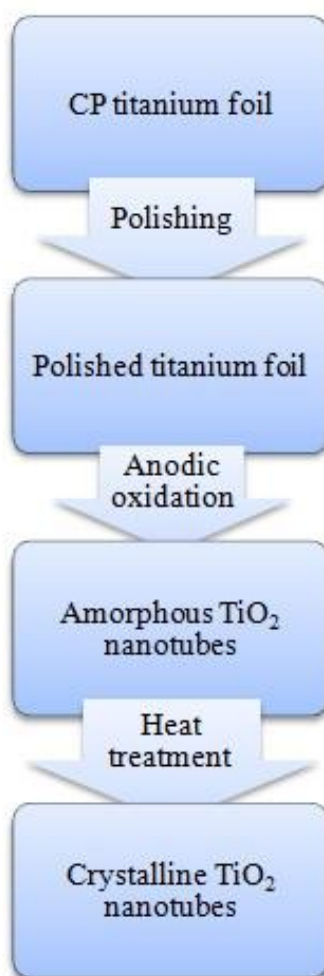


**Figure 6.1:** Flow chart of experimental procedure.

## 6.1 Surface Preparation

In order to prepare samples for anodic oxidation step, all specimens were prepared by standard metallographic grinding and polishing. All samples were ground with 600, 800, 1000 1200 and 2400 mesh SiC emery papers for 5 minutes. Afterwards, both surfaces of the ground samples were gently polished with 1  $\mu$  diamond abrasive paste on a MD Chem. cloth for 2 minutes. In order to eliminate a possible problem that could emerge from current density (because of extremely low thickness of titanium) on titanium anode, both surfaces of the samples were ground and polished, although only one surface is directly exposed to cathode material.

## 6.2 Anodic Oxidation

Titanium foils of 0.50 mm thickness and 99.2% purity were obtained from abcr GmbH Co. KG (Germany) and used as the anode in electrochemical anodization process. Cathode, the counter electrode, which was used in the experiments, was a platinum wire. All electrolytes were prepared from analytical grade chemicals and DI water. Anodization conditions varied between 10V – 40V for voltage and 10 and 40 minutes for duration. The anodizing voltage was kept constant during the entire process with a DC power supply and anodization was conducted at room temperature with magnetic stirring. Prior to anodization, titanium foils were cleaned by an acidic solution of 60% HNO<sub>3</sub> – 25% HF – 15% H<sub>2</sub>O to minimize any dirt on the surface and then dried in air. After anodization, both anode and cathode were washed in distilled water and dried in air. General view of the anodic oxidation equipment used in this thesis is given in Figure 6.2.



**Figure 6.2:** Anodic oxidation equipment used in this study.

### 6.3 Heat Treatment

To induce crystallization of amorphous TiO<sub>2</sub> nanotube arrays into crystalline TiO<sub>2</sub> phase (anatase or rutile) and to investigate the effect of annealing temperature and time on the structure of the nanotubes, annealing was carried out at several temperature and time combinations as given in Table 6.1.

**Table 6.1:** Annealing conditions applied to anodized CP titanium foils.

Annealing temperature (°C)	Annealing time (hour)
400	1
480	1, 2, 4, 8, 24
500	1
600	1
600	60
700	1

## 6.4 Characterization Tests

Characterization tests were performed on both unannealed and annealed oxidized samples. These tests include X-ray diffraction (XRD) analyses, scanning electron microscope (SEM) examinations, contact angle measurements and surface roughness measurements; some of them was only applied for unannealed and annealed samples.

### 6.4.1 X-ray diffraction analyses

Qualitative phase identification of anodized samples were held by X-ray diffractometer (XRD) (Bruker X-Ray Diffractometer, Figure 6.3.) with Cu  $K_{\alpha}$  radiation performed over angular ranges of  $2\theta = 20^{\circ}$ – $80^{\circ}$  with a step angle of  $0.02^{\circ}$ .



**Figure 6.3:** Bruker X-Ray Diffractometer.

### 6.4.2 Scanning electron microscope examinations

Surface morphologies of  $TiO_2$  nanotubes were investigated by JEOL JSM 7000F Field emission scanning electron microscope (FESEM), which operated at 10.0 kV with working distance (WD) 10.0 mm, as seen in Figure 6.4.





**Figure 6.4:** JEOL JSM 7000F Field Emission Scanning Electron Microscope.

#### **6.4.3 Contact angle measurements**

Contact angle measurements were performed by “KSV Cam 200 Contact Angle and Surface Tension Meter” equipment (as seen in Figure 6.5) in order to study surface wettability of the samples with distilled water. In all measurements, light phase was air and heavy phase was distilled water. Measurements were performed with a drop of 5  $\mu\text{l}$  distilled water.

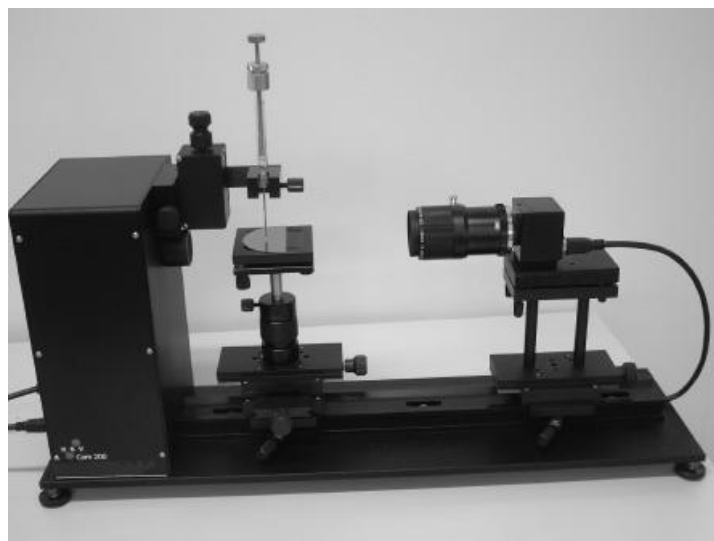


**Figure 6.5:** KSV Cam 200 Contact Angle and Surface Tension Meter.

#### **6.4.4 Surface roughness measurements**

Surface roughness of titania nanotubes was examined with Veeco Dektak 6M surface profilometer. Scan parameters of the profilometer were set as an applied force of 5 mg along a scan distance of 5000  $\mu\text{m}$  for 30 seconds duration.

## **7. RESULTS AND DISCUSSION**

In this chapter, results of experimental works and characterization studies are discussed.

### **7.1 Surface Morphologies of Titanium Dioxide Nanotubes**

Morphological characterization of titanium dioxide nanotubes were performed by SEM examination and the results were given and discussed in the following subsections with respect to the diameter and wall thickness of the nanotubes.

#### **7.1.1 Effect of voltage and time on nanotube diameter**

Anodized samples were divided into groups with respect to their anodization voltage applied. First group of samples were anodized under a voltage of 10V for four different times such as 5 minutes, 10 minutes, 20 minutes and 40 minutes. Figure 7.1 shows surface SEM micrographs of the samples anodized under a potential of 10V with respect to anodization time between 5 to 40 minutes. As shown in Figure 7.1, nanotube diameter of the samples anodized at 10V for 5 to 40 minutes varied between 40 nm and 60 nm and showed no significant difference with respect to the anodization time. It was also shown that sample anodized for 10 minutes at 10V exhibited better arrangement of nanotubes when compared to the other anodization times. This might be due to the fact nanotube formation rapidly progresses up to 10 minutes giving better arrangement of nanotubes. Beyond 10 minutes of anodization time, tubular structure and well defined arrangement of the nanotubes seems to be slightly deteriorated.

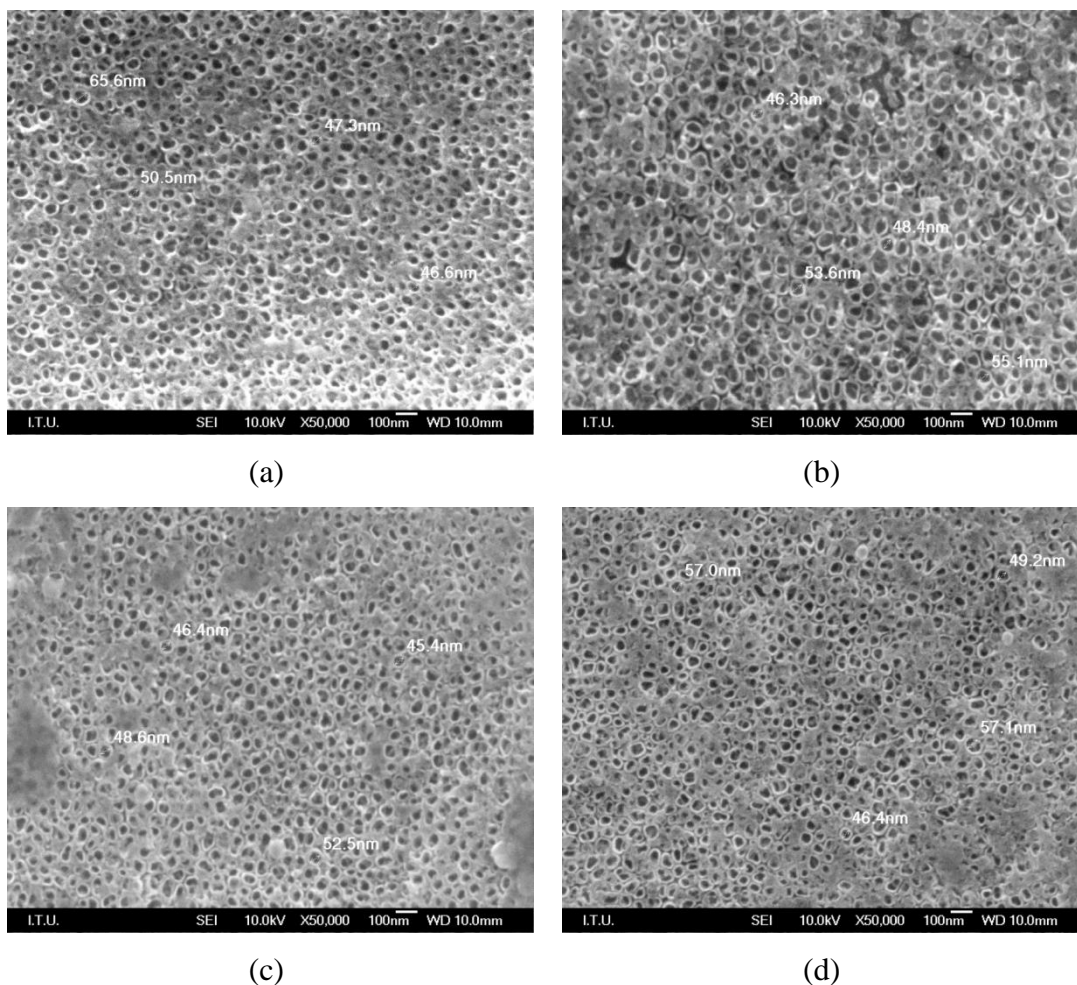


**Figure 7.1:** SEM images of TiO<sub>2</sub> structures anodized at 10V for (a) 5min, (b) 10 min, (c) 20 min and (d) 40 min.

Figure 7.2 shows surface SEM micrographs of the samples anodized under a potential of 20V with respect to anodization time between 5 to 40 minutes. As can be clearly seen in Fig 7.2, diameter of the nanotubes on the samples anodized at 20V were bigger when compared to those anodized at 10V, ranging from 45 nm to 110 nm with respect to the anodization time. For the samples anodized for 5 minutes, tube diameter varies between 45 nm and 80 nm. As the anodization time increases, nanotube diameter also increases to 60 nm to 85 nm, 80 nm to 110 nm and 50 nm to 100 nm with respect to anodization times of 10 minutes, 20 minutes and 40 minutes, respectively. Variation of nanotube diameter and the tangled shapes of nanotubes is the main result of increasing anodization time. In addition to increased nanotube diameter, nanotube arrays seem to be deformed in increasing extent with increasing anodization time. Formation of tangled shape morphology possibly is a result of

deterioration of nanotubes due to attack of  $F^-$  ions in the electrolyte to titanium at a higher voltage.

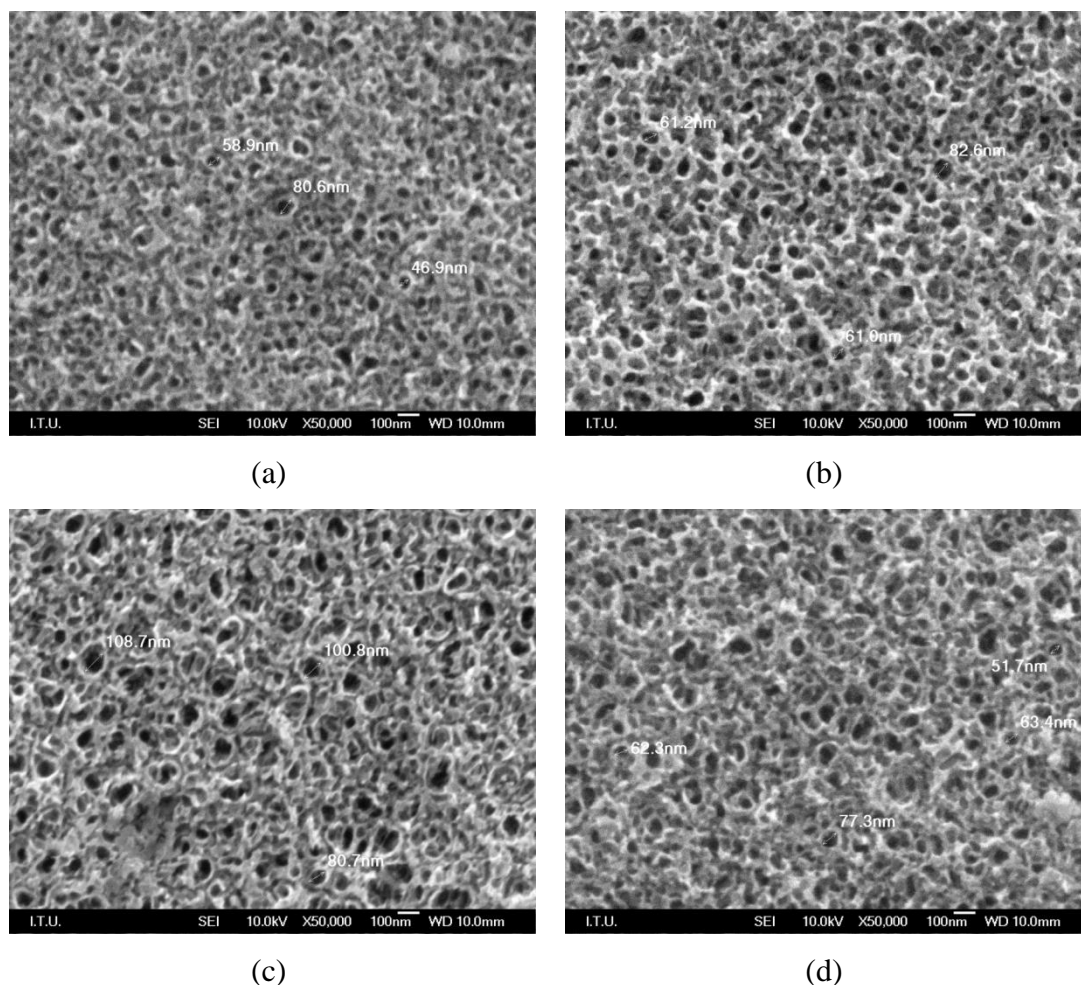


**Figure 7.2:** SEM images of  $TiO_2$  structures anodized at 20V for (a) 5min, (b) 10 min, (c) 20 min and (d) 40 min.

Figure 7.3 shows surface SEM micrographs of the samples anodized under a potential of 40V with respect to anodization time between 5 to 40 minutes. When compared to the samples anodized at 10V and 20V, samples anodized at 40 V have significantly different surface appearance in terms of size and shape of the nanotubes. Samples anodized at 40V generally had an etch like surface morphology regardless of the anodization time, which becomes more apparent for longer anodization times. For the sample anodized at 40V for 5 min, nanotubes starts to deteriorate leaving behind a nanopored surface appearance instead of regular nanotube arrangement. For longer anodization times, surface became rougher indicating almost complete disappear of the nanotubes. Surface SEM examinations performed on the samples anodized at 10V, 20V and 40V revealed that anodization

voltage and anodization time both have a strong influence on surface morphology and regular arrangement of nanotubes.

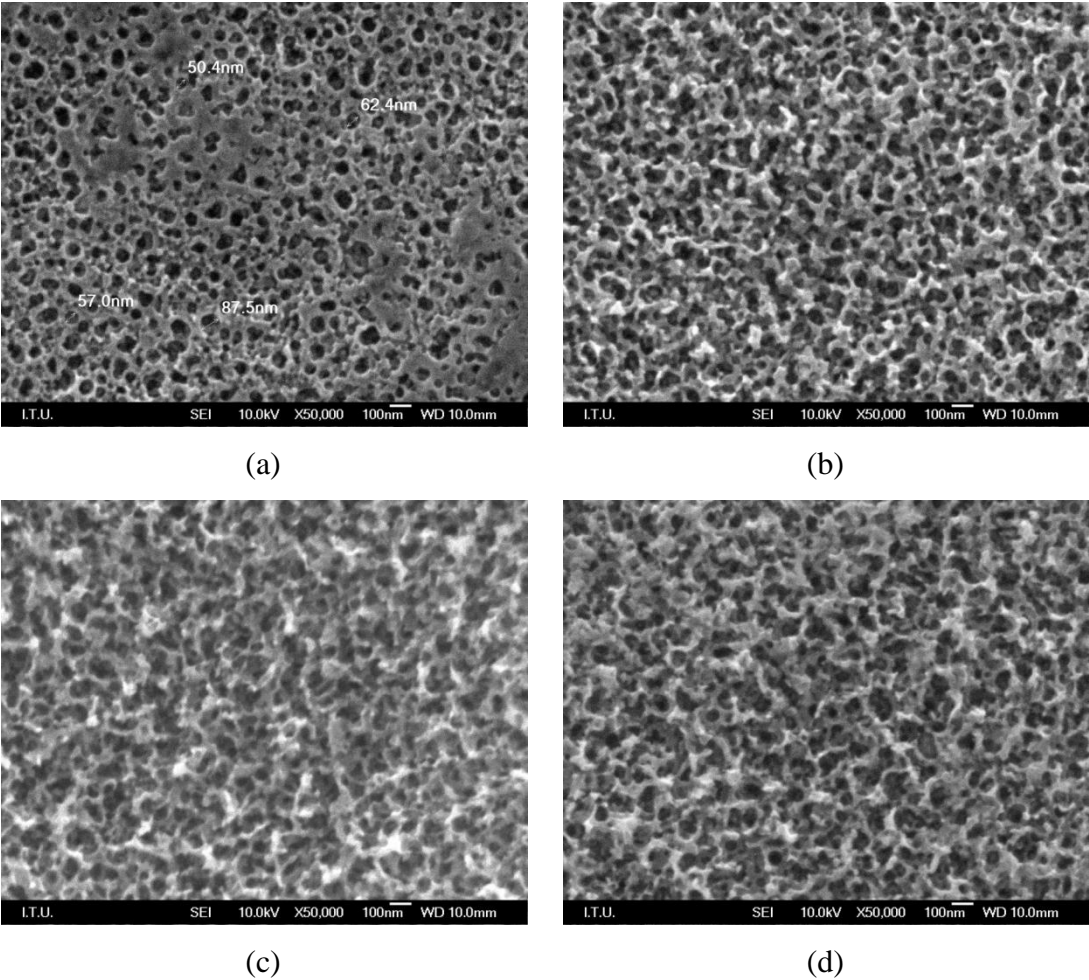
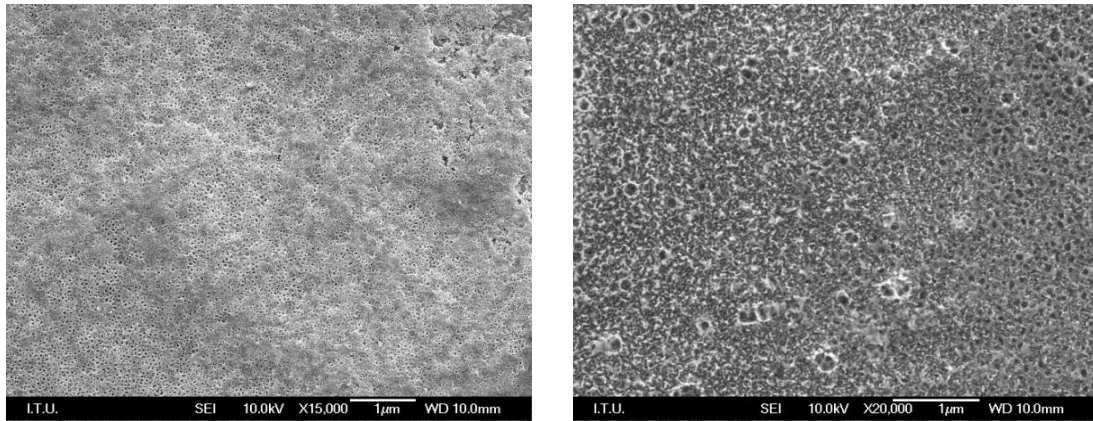


**Figure 7.3:** SEM images of TiO<sub>2</sub> structures anodized at 40V for (a) 5min, (b) 10 min, (c) 20 min and (d) 40 min.

In Figure 7.4, samples anodized at 10V for 40 minutes and 40V for 5 minutes were compared. It should be noted that remarkable coarsening is evident on the surface of the sample anodized at 40V.

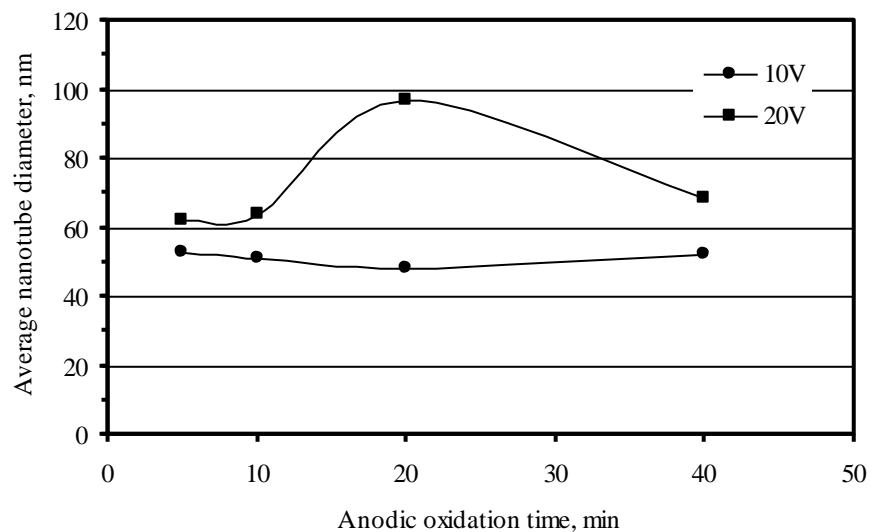


(a)

(b)

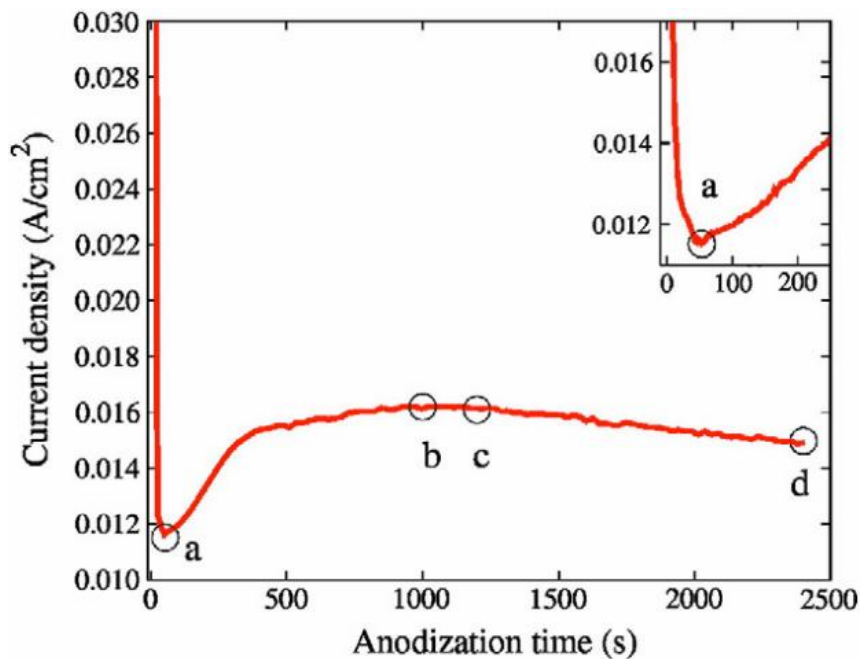
**Figure 7.4:** Surface morphologies of samples anodized at (a) 10V for 40 minutes and (b) 40V for 5 minutes.

Figure 7.5 shows average diameter of the nanotubes on the samples anodized at 10V and 20V. As already mentioned, average nanotube diameter on the samples anodized at 10V was in the range of 40 – 50 nm and does not display any systematic variation with respect to the anodization time. On the other hand, for the samples anodized at 40V, average nanotube diameter was about 60 nm for the sample anodized for 5 minutes, reached to about 100 nm for the sample anodized for 20 minutes and then decreased to 70 nm for the sample anodized for 40 minutes. From these datas, it was concluded that anodization voltage and anodization time are both strong parameters affecting nanotube diameter. On the other hand, further increase in voltage level and anodization time has a deteriorating effect on nanotube morphology.



**Figure 7.5:** Variation of average nanotube diameter with anodization time.

There is an example of current density - anodization time diagram, which is retrieved from literature, as seen in Figure 7.6 [38]. As explained before, first step of nanotube formation is the formation of oxide layer, which is followed by the pit formation. At the first seconds of anodic oxidation, current density decreases in a fast trend to the bottom point (a) and this is because of pit formation on oxide layer. After then, pits turn into pores with an increasing trend (b) which will become highly ordered nanotube arrays later. At point (b), maximum nanotube diameter is achieved and so in steady state (c), pore diameters do not depend on anodization time. If the anodization process is continued, (d) current density will start to decrease by time because of insufficient metal cations providing electrochemical dissolution.



**Figure 7.6:** Typical current density - anodization time diagram [38].

A similar variation of current density with anodization time was also observed for the sample anodized at 10V for 10 minutes, which yields more uniform distribution of nanotubes on the surface. Anodization time of 10 minutes was corresponding to a stage of constant current density as shown in Figure 7.7, which was in agreement with the explanation given in the literature [38].



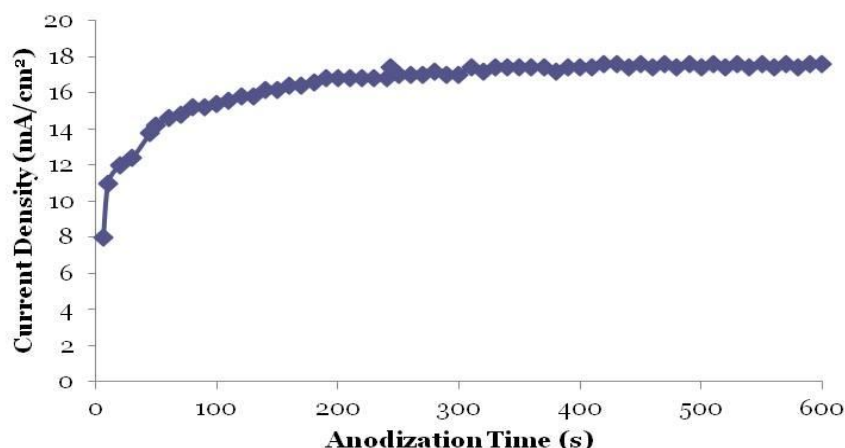


**Figure 7.7:** Current density - anodization time diagram of sample anodized at 10V for 10 minutes.

A linear evolution of nanotube diameter observed with a high slope until 100 seconds. The trend is weak between 100 - 400 seconds and finally at 600 seconds, maximum diameter is achieved for the sample anodized 10V for 10 minutes.

### 7.1.2 Wall thickness variation

Wall thickness of TiO<sub>2</sub> nanotubes has been typically reported to be a few tens of nanometers [23]. For some applications of titanium dioxide nanotubes, such as hydrogen sensing and photocatalytic properties, wall thickness is a very important parameter. However, there is only limited data available regarding the control of nanotube wall thickness as already mentioned in Chapter 5. It was reported in the literature that wall thickness of nanotubes might vary depending on type of the electrolyte. However, in this study, one type of electrolyte (aqueous solution of 1% HF) was used for all of the anodization works, which is unlikely to have an effect on wall thickness.

Figure 7.8 shows high magnification SEM micrographs of the samples anodized at 10V for 10 minutes and 20 minutes. From these micrographs, nanotube wall thickness was measured in the range of 8-10 nm for both samples anodized at the same voltage level for different times. This indicates that anodization time has no significant effect on wall thickness, as expected.

These low wall thickness values make the samples anodized at 10V appropriate for hydrogen sensing and photocatalytic applications as long as low nanotube diameter is

achieved [23]. Samples anodized at 20V and 40V are not considered for wall thickness measurements, due to their morphologies.

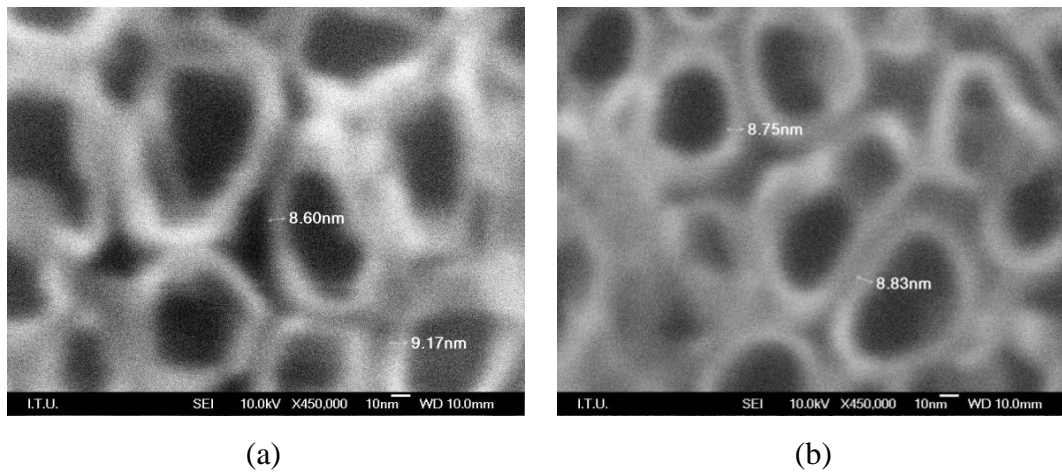


**Figure 7.8:** SEM images showing wall thickness of titanium dioxide nanotubes for samples anodized at 10V for (a) 10 min. and (b) 20 min.

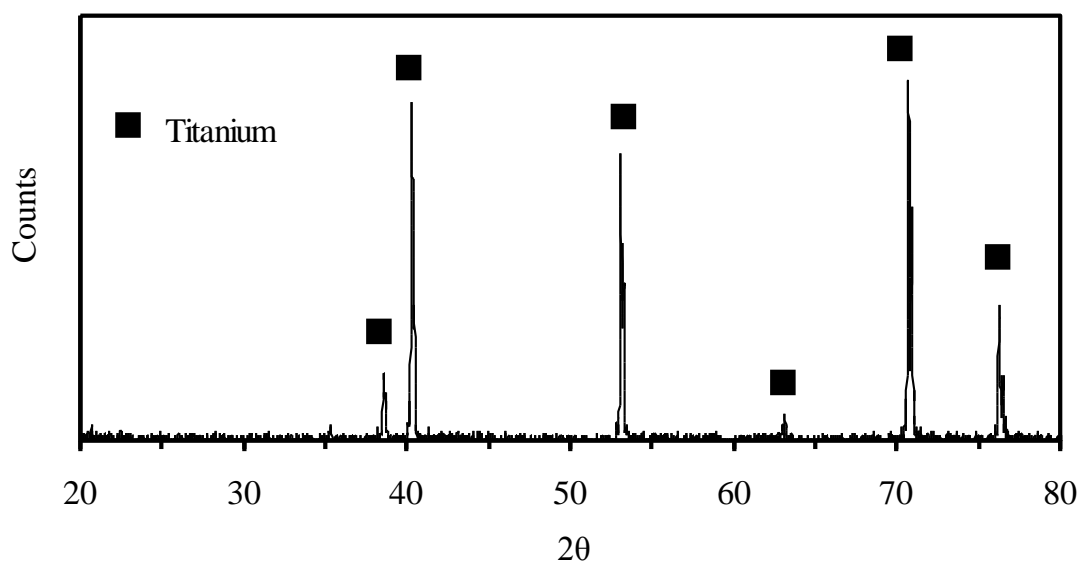
## 7.2 Structural Analysis of Titanium Dioxide Nanotubes

X-ray diffractometry was used in order to make a qualitative analysis of structure of the nanotube morphology. According to literature survey [25, 39, 40], XRD patterns are mostly obtained for the  $2\theta$  range of  $20^\circ - 80^\circ$ , where  $\alpha$  titanium (base metal lying under nanotube arrays) and  $\text{TiO}_2$  peaks are located, can be obtained.

### 7.2.1 XRD patterns of unannealed samples

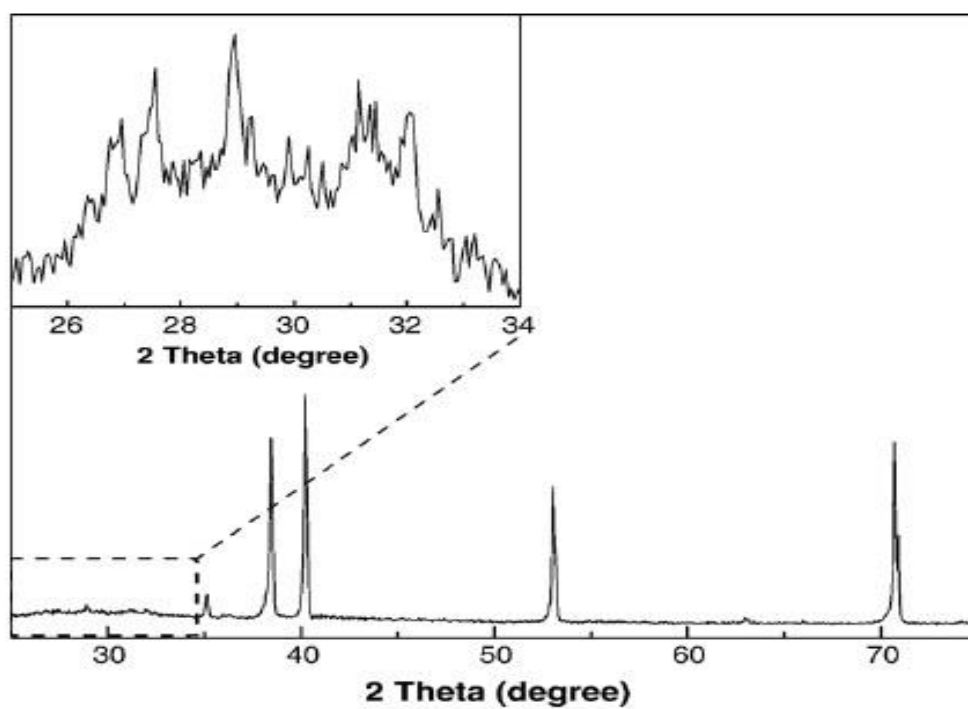
For all unannealed samples,  $\alpha$  titanium peaks were observed at  $2\theta$  of  $39^\circ$ ,  $41^\circ$ ,  $54^\circ$ ,  $71^\circ$  and  $77^\circ$ . Due to amorphous structure of titanium dioxide nanotubes, no  $\text{TiO}_2$  peaks were seen in the patterns, as expected. All the unannealed anodized foils have similar XRD patterns consisting of  $\alpha$  titanium. XRD patterns of all the samples anodized at 10V, 20V and 40V were given in APPENDIX A, in Figure A.1, A.2 and A.3, respectively.

Figure 7.9 shows XRD pattern of the unannealed sample anodized at 10V for 10 minutes. In the figure, black squares indicate  $\alpha$ -titanium.



**Figure 7.9:** XRD pattern of titanium foil anodized at 10V for 10 minutes.

Figure 7.10, which is retrieved from literature, shows that XRD pattern of unannealed anodized CP titanium sample, which indicates  $\alpha$  titanium peaks and amorphous nature of the structure [39]. XRD pattern obtained in this thesis (Figure 7.9) were in good agreement with that reported in the literature.



**Figure 7.10:** XRD pattern retrieved from literature [39].

### 7.2.2 XRD patterns of annealed samples

Annealing treatment was applied to the samples anodized at 10V for 10 minutes, which has better arrangement of the nanotubes throughout the surface. Upon annealing, structure transforms from amorphous to crystalline comprising anatase and rutile modifications of TiO<sub>2</sub> in different intensities, as expected. As an example, XRD pattern of the sample annealed at 480°C for 24 hours is given in Figure 7.11. XRD patterns of the other samples annealed at 400°C, 500°C, 600°C and 700°C for various times are given in Figure A.4 and A.5 in APPENDIX A. XRD pattern of the sample annealed at 480°C for 24 hours shows that nanotube structure contains anatase and rutile peaks beside  $\alpha$ -titanium peaks coming from the underlying CP titanium. As shown in Figure A.4, as the annealing time increases at 480°C, anatase and rutile peaks become more visible; especially for annealing time of 24 hours.

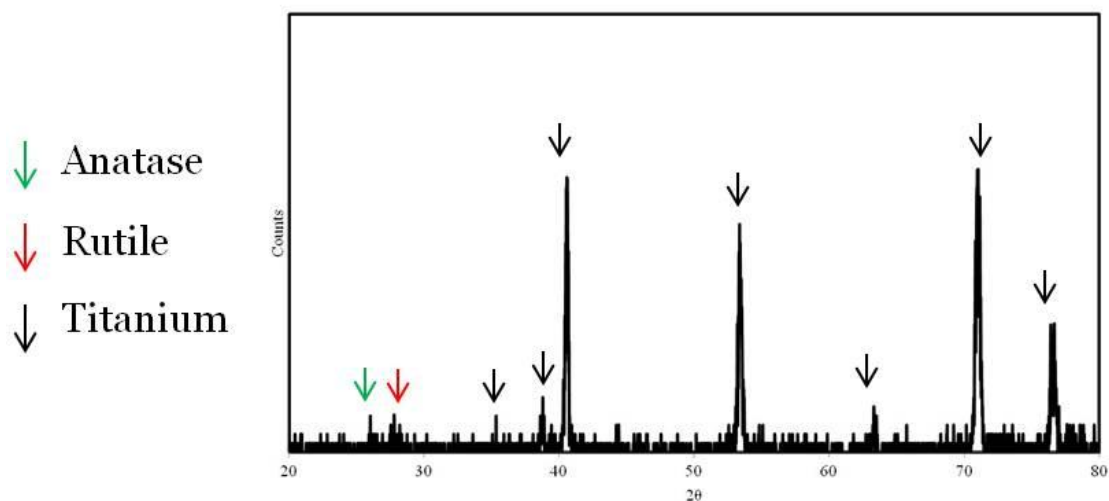


**Figure 7.11:** XRD pattern of sample annealed at 480°C for 24 hours.

On the other hand, XRD patterns of the samples annealed at 400°C and 500°C display weak anatase and rutile peaks between  $2\theta = 20^\circ$  and  $40^\circ$  interval. As the annealing temperature is increased to 600°C, rutile peaks becomes more visible along with weak anatase peak. However, when the annealing time is increased from 1 h to 60 h at 600°C, anatase peak disappears and intensity of rutile peaks increases. At 700°C, only rutile peaks were observed in XRD patterns as shown in Figure A.5.

### 7.3 Analysis of Contact Angle Measurements

Relation between cohesion forces (attraction forces between liquid molecules) and adhesion forces (attraction forces between liquid and solid) determines the wettability of any surface, which is also known as contact angle.

Contact angle measurements are important in that it provides some information about suitability of TiO<sub>2</sub> nanotube arrays for biomedical applications. Wettability of TiO<sub>2</sub> nanotube arrays is not only important for biomedical applications, but also important for drug delivery applications; which is another important area of application of these structures. This is a result of nanotube arrays having high surface area and volume providing drug emission [23].

As seen in Figure 7.12, contact angle measurements were performed by a water droplet dropped onto an anodized sample.

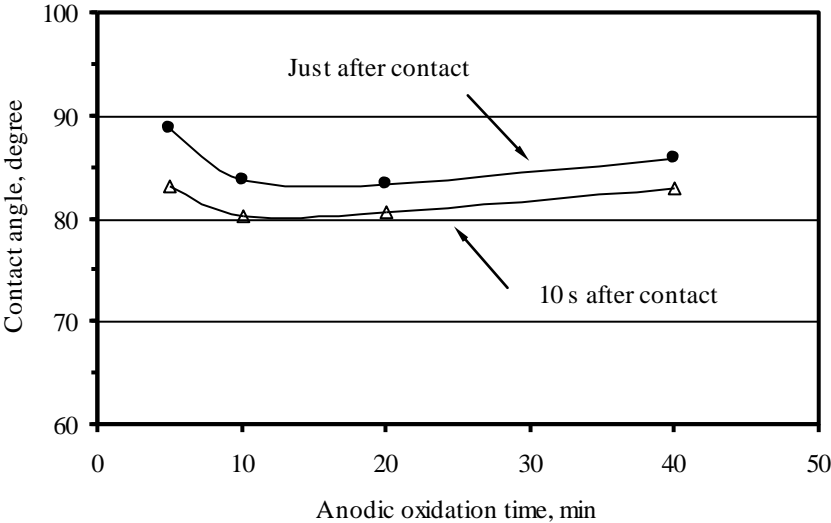


**Figure 7.12:** View of a water droplet 10s after dropped on CP titanium sample anodized at 10V for 10 minutes

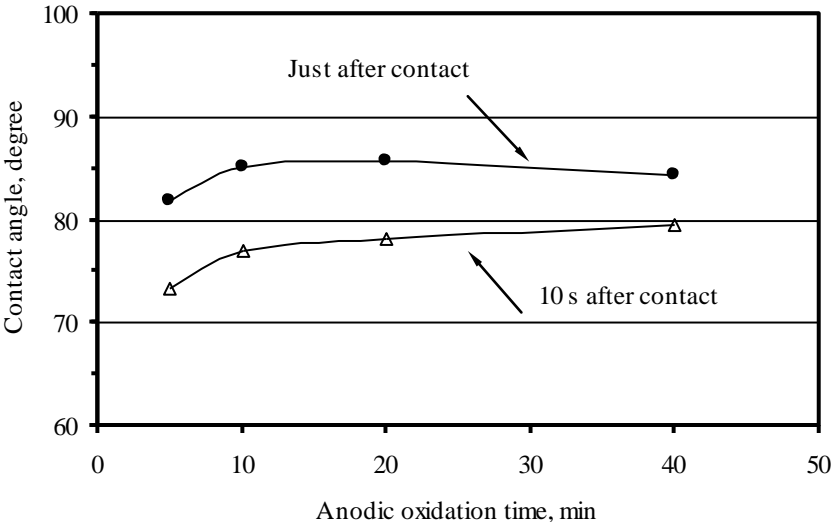
Samples anodized at 10V and 20V were considered for contact angle measurements because of their surface structures with nanotube morphology. However, samples anodized at 40V potential were also evaluated in order to make a comparison between surfaces with highly ordered nanotubes and etched-like surface.

Figure 7.13 and Figure 7.14 show the contact angle measurements of the samples anodized at 10V and 20V with anodization time, respectively. As the anodization voltage was increased from 10V to 20V, contact angles were decreased indicating that water could be spread easier over to surface anodized at 20V. On the other hand,

contact angles followed an increasing trend with the increasing anodization time at a constant applied voltage.



**Figure 7.13:** Contact angle measurements of samples anodized at 10V as a function of anodization time.



**Figure 7.14:** Contact angle measurements of samples anodized at 20V as a function of anodization time.

Contact angle values measured just after the contact are very close to 90° and almost equal to each other for both anodization voltage (10V and 20V). Although contact angles values decreased 10s after contact for both samples, decrement is smaller for the sample anodized at 10V, which is closer to the values at the time of contact. This

means that the sample anodized at 10V has less wettability when compared to that of the sample anodized at 20V. Ability to control wettability is reported to be useful for biomedical applications [38].

Figure 7.15 shows contact angle values as a function of anodization time at 40V, which were lower when compared to those of the samples anodized at 10V and 20V.

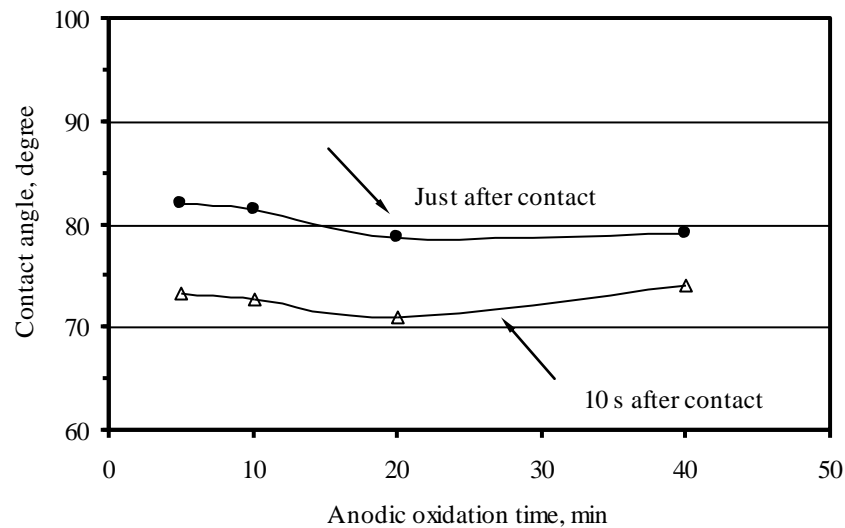


**Figure 7.15:** Contact angle measurements of samples anodized at 40V as a function of anodization time.

Contact angle values measured on all the samples clearly suggest that well arranged nanotube formation decreased wettability by increasing contact angle. This means that lower anodization voltage provides cohesion forces superiority over adhesion forces and vice versa.

#### 7.4 Analysis of Surface Roughness Measurements

Anodization at different voltage levels generates different morphologies at the surface. Relatively lower voltage forms regular nanotube arrays, while deformation of these nanotube arrays takes place due to dissolution of  $\text{TiO}_2$  structures when the anodization voltage is increased. Surface roughness, is a measure of surface texture and quantified by the vertical deviations of a real surface from its ideal form. Higher deviations indicate high surface roughness values, as well as lower deviations indicate smoother surfaces [41]. In surface roughness measurements, there are number of surface parameters used and these represent different morphological

features of the surface. Most commonly used surface roughness is arithmetical mean roughness ( $R_a$ ), shortly “arithmetic average” with the unit of  $\mu\text{m}$ .

As the anodization voltage increased, mean surface roughness increased accordingly. An increase in mean surface roughness with increasing anodization voltage is possibly arisen from the dissolution of nanotube arrays in different rates. In addition, mean surface roughness can also be correlated with contact angle measurement in that rougher surfaces provide lower contact angle values. On the other hand, there is not a systematic variation in mean surface roughness with anodization time. Figure 7.16 shows variation of mean surface roughness with anodization time for different anodization voltage.

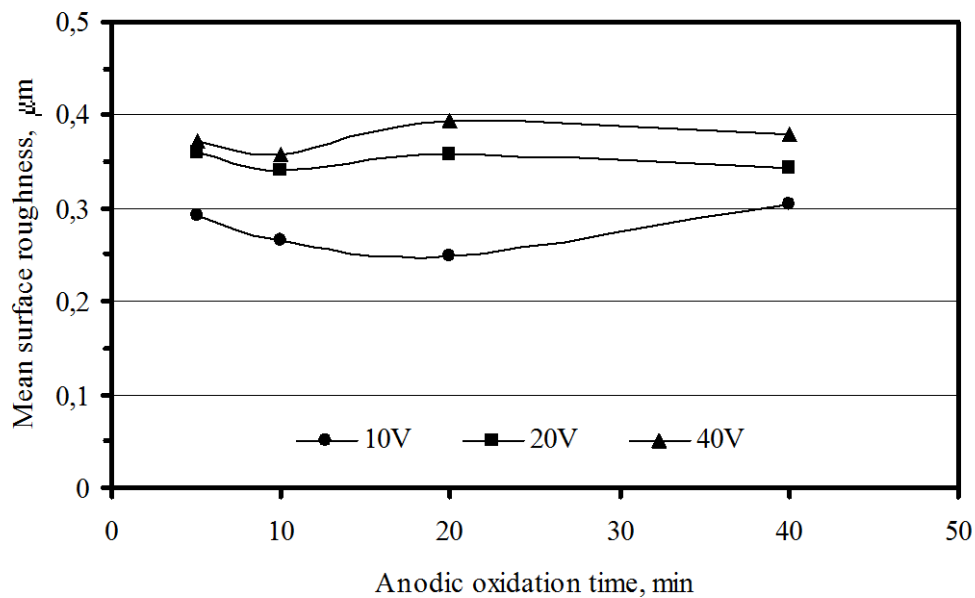


**Figure 7.16:** Variation of mean surface roughness as a function of anodization time for different anodization voltages.

### 7.5 Evaluation of $\text{TiO}_2$ Nanotube Structures for Selected Applications

In order to provide hydrogen gas sensing property to anodized amorphous structured titanium dioxide nanotubes, controlled heat treatment must be applied, in order to obtain a crystalline structure. For this reason,  $\text{TiO}_2$  nanotube arrays are annealed in a temperature interval that makes the material containing both anatase and rutile phases.



Phase transformations in titanium dioxide nanotubes can be explained as; structure annealed at 300°C having an unstable phase of anatase nucleation. As this temperature increases towards 500°C, a combination of anatase - rutile phases is observed. Anatase phase is at nanotube walls and rutile phase is at nanotube/metal interface. As a result, this temperature range can be count ideal for hydrogen sensing. The main reason of this temperature range and anatase - rutile mixture's availability for hydrogen sensing is, due to the different structures of these two phases. Small nucleus size of anatase crystalline (<38 nm for anatase, while 240 nm for rutile) and c/a ratio's superiority over rutile crystalline for four times provides hydrogen atoms diffuse into the structure. However, if all the system had the anatase structure, then there would not be a difference between nanotube and metal/nanotube interface to sense hydrogen atoms. This would result as an ineffective approach [42].

Further increase of annealing temperature (about 600°C), results with a fully rutine transformed structure; which is undesired for hydrogen sensing applications not only because of the deformed structure of nanotubes due to high temperatures, but also nanotube walls only consisting of rutile phase. Figure 7.17 shows the crystallization steps of titanium dioxide nanotubes.

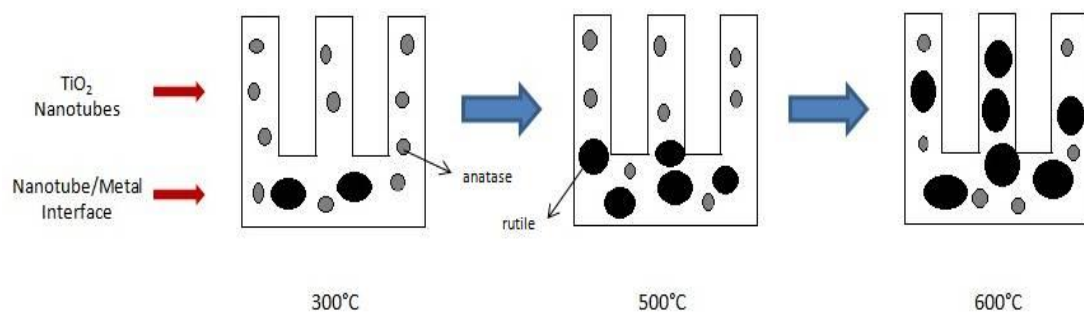


**Figure 7.17:** Schematic representation of crystallization steps of TiO<sub>2</sub> nanotubes.

Length and wall thickness of titania nanotubes have important properties for hydrogen gas sensing applications which requires high surface area. A crystalline structure, lower wall thickness and increased length are the desired parameters for TiO<sub>2</sub> nanotube arrays with good hydrogen sensing properties. It was found that the hydrogen sensitivity of the nanotubes was highly dependent upon nanotube diameter, with 22 nm pore size nanotubes being about 200 times more sensitive than 76 nm pore size nanotubes, although the smaller pore size nanotubes have a larger surface

area by only 30%. It that should be noted, the main mechanism behind enhancement of conductance in TiO<sub>2</sub> nanotubes with hydrogen exposure is, neither the reduction of TiO<sub>2</sub> lattice nor removal of chemisorbed oxygen from the nanotube surface by the hydrogen. The dominant mechanism behind the electrical behavior of the titanium dioxide nanotubes is chemisorption of the spilled-over hydrogen atoms on the nanotube surface, which make a partial charge transfer to the TiO<sub>2</sub> structure, thereby creating an electron accumulation layer on the nanotube surface that enhances the electrical conductance [23].

Photoelectrolysis is the term used to describe semiconductor-based water splitting by the use of a photoelectrochemical cell (PEC). One approach is to couple a photovoltaic system and an electrolyzer as a single system. Photovoltaic cells can be combined in series to generate the potential needed to split water and then connected to H<sub>2</sub> and O<sub>2</sub> producing electrodes. With semiconductor–liquid junctions, the water splitting potential is generated directly at the semiconductor–liquid interface. The ability of a semiconductor photoelectrode to drive either the oxidation of water to O<sub>2</sub>, or the reduction of water to H<sub>2</sub>, or the entire water splitting reaction is determined by its band gap and the position of the valence and conduction band edges relative to the water redox reactions. Figure 7.18 shows the schematic representation of a photoelectrolysis cell [23].

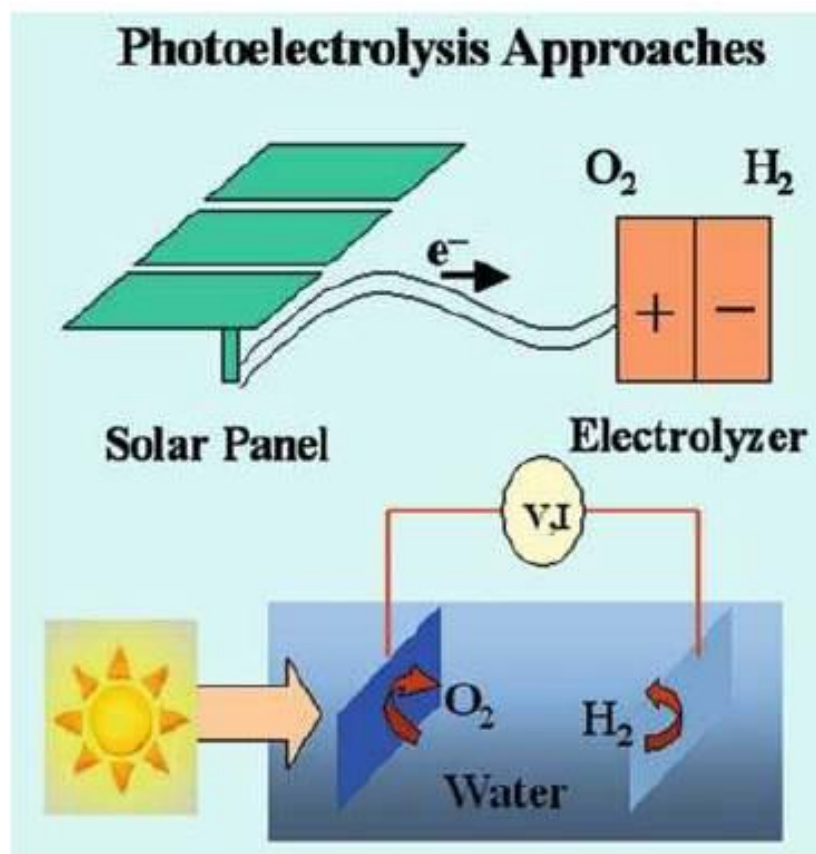


**Figure 7.18:** Schematic representation of PEC [23].

A photoelectrochemical (PEC) system combines the harvesting of solar energy with electrolysis of water. When a semiconductor of proper characteristics is immersed in an aqueous electrolyte and irradiated with sunlight, sufficient energy is generated to split water into hydrogen and oxygen. However, there are three major challenges for the solar production of hydrogen:

- (1) Stability. Metal oxides are the most photochemically stable semiconductors in aqueous solution, but their band gaps are either too large ( $\sim 3$  eV) to absorb a significant fraction of incident solar energy, or their semiconductor characteristics (e.g., charge transport) are poor.
- (2) Band-gap. Considering the water splitting energy of 1.23 eV and overpotential losses, the semiconductor should have a bandgap greater than 1.7 eV. However, semiconductors with such relatively low bandgaps have been found to lack stability during water splitting.
- (3) Energy levels. Even though a semiconductor electrode may generate sufficient energy to drive an electrochemical reaction, the band edge

positions may prevent it from doing water splitting. For spontaneous water splitting, water oxidation and reduction potentials must lie between the valence and conduction band edges.

TiO<sub>2</sub> nanotube array architecture possesses high surface to volume ratios, which enables a large internal surface area to be in intimate contact with the electrolyte, and excellent charge transfer properties. However, TiO<sub>2</sub> is responsive to UV light, which accounts for only a small fraction (~4%) of the sun's energy. Visible light comprises approximately 45% hence any shift in the optical response of TiO<sub>2</sub> from the UV to the visible spectral range while maintaining the intrinsic properties of TiO<sub>2</sub>, for example the excellent charge transfer properties and photocorrosion stability, will have a positive impact on the photocatalytic and photoelectrochemical utility of the material. Finally, the higher electrochemical current density of the nanotube arrays is directly related to the higher surface area. This can be achieved by high nanotube length and low wall thickness. Not only shape of nanotubes, but also crystal structure has effects on photoelectrolysis properties. The increased crystallinity of the nanotubes annealed at elevated temperatures reduces the number of grain boundaries, improves connectivity between grains and eliminates any amorphous regions that provide defects acting as carrier recombination centers [23].

## 8. CONCLUSIONS AND RECOMMENDATIONS

In this study, CP titanium foil was anodized in an aqueous solution 1%HF at various voltage level for various times to produce a nanotube morphology on the surface and the anodized samples were annealed at various temperature and time combinations. Characterization works including qualitative XRD analysis and SEM examinations led to the following conclusions:

1. Highly ordered nanotube morphology was produced on the surface of CP titanium surface as verified by SEM examinations.
2. XRD analysis reveal that as anodized surfaces have an amorphous structure with a titanium peaks coming from the underlying titanium foil, which indicates that no impurity or phase evolved during anodic oxidation process.
3. Anodization voltage has a strong influence on the nanotube morphology. SEM examinations reveal that, optimum morphology with more regular arrangement of nanotubes with an average diameter 50 nm are achieved by anodizing the sample at 10V for 10 minutes. When the anodization voltage is increased to 20V, even though surface has still the nanotube morphology with an increased average diameter of 75 nm, regular arrangement of the nanotube arrays started to be deteriorated. When the potential is further increased to 40V, regular nanotube morphology almost disappear and the surface gets rougher exhibiting an etch like morphology especially for longer anodization times, possibly as a result of breakdown of nanotube arrays.
4. As the anodization time increases, on the other hand, there is no significant deterioration on the morphology for the samples anodized at 10V. When the samples are anodized at 20V, nanotube diameter increases from 60 nm to 100 nm up to 20 minutes and then slightly decrease to ~70 nm. When the anodization voltage is increased to 40V, surface becomes increasingly deteriorated with increasing anodization time.
5. There is no wall thickness variation observed for titanium dioxide nanotubes with the effect of anodization time for the samples anodized at 10V. Same

wall thickness values of 8 - 9 nm achieved both for 10 minutes and 20 minutes anodizing times.

6. Annealing at 400°C to 700°C in air for various times provides transformation of the amorphous structure into crystalline structure. At lower annealing temperatures (400°C, 480°C and 500°C) structure consists of anatase and rutile modifications of TiO<sub>2</sub>. As the annealing temperature increases to 600°C and 700°C rutile peaks become more apparent with almost complete disappear of anatase phase.
7. In the view point of wettability, contact angle measurements revealed that, samples anodized at lower voltage levels have higher contact angle values, indication lower wettability. As the anodization voltage increases contact angle values are decreased accordingly, possibly due to deterioration of the nanotube morphology.
8. Means surface roughness values of the samples exhibit that surfaces become increasingly rougher with increasing anodization voltage. On the other hand, anodization time does not seem to have a strong influence on mean surface roughness of the samples.

## REFERENCES

- [1] **Lütjering, G., and Williams, J. C.** (2007). Engineering Materials and Process: Titanium (2nd Edition). Springer.
- [2] **Kasuga, T., Hiramatsu, M., Hoson, A., Sekino, T., Niihara, K.** (1998). Formation of Titanium Oxide Nanotube. *Langmuir*, 14, 3160-3163.
- [3] **Gong, D., Grimes, C. A., Varghese, O. K., Dickey, E. C.** (2001). Titanium Oxide Nanotube Arrays Prepared by Anodic Oxidation. *Journal of Materials Research*, 16, 3331-3334.
- [4] **Bavykin, D. V., and Walsh, F. C.** (2010). Titanate and Titania Nanotubes Synthesis, Properties and Applications. RSC Publishing, UK.
- [5] **Higgins, R. A.** (2006). Materials for Engineers and Technicians (4th Edition). Newnes.
- [6] **Bomberger, H. B., Froes, F. H., Morton, P. H.** (1985). Titanium Technology: Present Status and Future Trends. TDA, Dayton, USA.
- [7] **Eylon, D., and Seagle, S.R.** (2000). Titanium '99, Science and Technology. CRISM Prometey, Russia.
- [8] **Metals Handbook Volume 2.** Properties and Selection: Nonferrous Alloys and Special Purpose Materials. ASM International, USA.
- [9] **Donachie, M. J.** (2000). Titanium: A Technical Guide (2nd Edition). ASM International.
- [10] **Polmear, I. J.** (2006). Light Alloys: From Traditional Alloys to Nanocrystals (4th Edition). Elsevier.
- [11] **Leyens, C., and Peters, M.** (2003). Titanium and Titanium Alloys: Fundamentals and Applications. Wiley-VCH.
- [12] **Çakır, D.** (2008). Titanium Dioxide Nanostructures for Photocatalytic and Photovoltaic Applications. *Ph.D. Thesis*, Bilkent University, Turkey.
- [13] **Sekino T.** (2010). Synthesis and Applications of Titanium Oxide Nanotubes. *Topics in Applied Physics*, 117, 17-32.
- [14] **Iijima, S.** (1991). Helical Microtubules of Graphitic Carbon. *Nature*, 354, 56-58.
- [15] **Gogotsi, Y.** (2006). Nanotubes and Nanofibers. CRC Press, USA.
- [16] **Harris, P. J.** (2009). Carbon Nanotube Science: Synthesis, Properties and Applications. Cambridge University Press, UK.
- [17] **Haddon, R., and Chow, S.** (1999). Hybridization As a Metric for the Reaction Coordinate of the Chemical Reaction: Concert in Chemical Reactions. *Pure and Applied Chemistry*, 71, 289-294.

- [18] **Yakobson, B.** (1998). Mechanical Relaxation and Intramolecular Plasticity in Carbon Nanotubes. *Applied Physics Letters*, 72, 918-920.
- [19] **Treacy, M., Ebbesen, T., Gibson, J.** (1996). Exceptionally High Young's Modulus Observed for Individual Carbon Nanotubes. *Nature*, 381, 678-680.
- [20] **Keller, F., and Hunter M.** (1953). Structural Features of Oxide Coatings on Aluminum. *Journal of Electrochemistry Society*, 100, 411-419.
- [21] **Rao, C. N. R., and Govindaraj, A.** (2005). Nanotubes and Nanowires. RSC Publishing, UK.
- [22] **Han, S. C., Doh, J. M., Yoon, J. K., Kim, G. H., Byun, Y. J., Han, S. H.** (2008). Highly Ordered TiO<sub>2</sub> Nanotube Arrays Prepared by a Multi-Step Anodic Oxidation Process. *Metals and Materials International*, 15, 493-499.
- [23] **Grimes, C. A., and Mor G. K.** (2009). TiO<sub>2</sub> Nanotube Arrays: Synthesis, Properties and Applications. Springer Science, USA.
- [24] **Allam, N. K., and Grimes, C. A.** (2008). Effect of Cathode Material on the Morphology and Photoelectrochemical Properties of Vertically Oriented TiO<sub>2</sub> Nanotube Arrays. *Solar Energy Materials Solar Cells*, 92, 1468-1475.
- [25] **Zhao, J., Xiaohui, W., Chen, R., Li, L.** (2005). Fabrication of Titanium Oxide Nanotube Arrays by Anodic Oxidation. *Solid State Communications*, 134, 705-710.
- [26] **Parkhutik, V. P., and Shershulsky, V. I.** (1992). Theoretical Modeling of Porous Oxide-Growth on Aluminum. *Journal Physics*, 25, 1258-1263.
- [27] **Zwilling, V., Aucouturier, M., Darque-Ceretti, E.** (1999). Anodic Oxidation of Titanium and TA6V Alloy in Chromic Media. *Electrochimica Acta*, 45, 921-929.
- [28] **Zwilling, V., Boutry-Forveille A., Aucouturier, M., Darque-Ceretti, E., David, D.** (1999). Structure and Physicochemistry of Anodic Oxide Films on Titanium and TA6V Alloy. *Surface and Interface Analysis*, 27, 629-637.
- [29] **Macdonald, D.** (1993). On the Formation of Voids in Anodic Oxide-films on Aluminum. *Journal Electrochemical Society*, 140, L27-L30.
- [30] **Siejka, J., and Ortega, C.** (1977). O-18 Study of Field-assisted Pore Formation in Compact Anodic Oxide-films on Aluminum. *Journal Electrochemical Society: Solid State Science Technologies*, 124, 883-891.
- [31] **Thompson, G.E.** (1997). Porous Anodic Alumina: Fabrication, Characterization and Applications. *Thin Solid Films*, 297, 192-201.
- [32] **Jaroenworoluck, A., Regonini, D., Bowen, C. R., Stevens, R., Macro, D.A.** (2007). Micro and Nanostructure of TiO<sub>2</sub> Anodised Films Prepared in a Fluorine-containing Electrolyte. *Journal of Materials Science*, 42, 6729-6734.



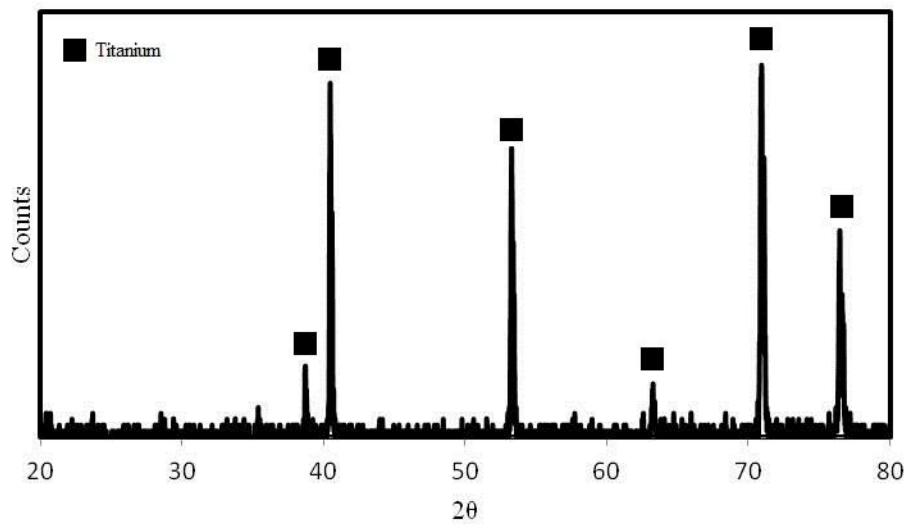
- [33] **Lohrengel, M.** (1993). Thin Anodic Oxide Layers on Aluminum and Other Valve Metals. *Materials and Science Engineering R*, 11, 243-294.
- [34] **Hwang, B. J., and Hwang, J. R.** (1993). Kinetic-model of Anodic-oxidation of Titanium in Sulfuric Acid. *Journal of Applied Electrochemistry*, 2, 1056-1062.
- [35] **Sul, Y. T., Johansson, C. B., Jeong, Y., Albrektsson, T.** (2001). The Electrochemical Oxide Growth Behaviour on Titanium in Acid and Alkaline Electrolytes. *Medical Engineering Physics*, 23, 329-346.
- [36] **Chen, S. G., Paulose, M., Ruan, C., Mor, G. K., Varghese, O. K., Kouzoudis, D., Grimes, C. A.** (2006). Electrochemically Synthesized CdS Nanoparticle-modified TiO<sub>2</sub> Nanotube-array Photoelectrodes: Preparation, Characterization and Application to Photoelectrochemical cells. *Journal of Photochemistry & Photobiology*, 177, 177-184.
- [37] **Mor, G. K., Varghese, O., Paulose, M., Mukherjee, N., Grimes, C. A.** (2003). Fabrication of Tapered, Conical-shaped Titania Nanotubes. *Journal of Materials Research*, 18, 2588-2593.
- [38] **Chassot, E., and Raspal, V.** (2010). Tunable Functionality and Toxicity Studies of Titanium Dioxide Nanotube Layers. *Thin Solid Films*, 519, 2564-2568.
- [39] **Chen, X., Schriver, M., Suen, T., Mao, S. S.** (2007). Fabrication of 10 nm Diameter TiO<sub>2</sub> Nanotube Arrays by Titanium Anodization. *Thin Solid Films*, 515, 8511-8514.
- [40] **Awitor, K. O., Rafqah, S., Geranton, G., Sibaud, Y.** (2008). Photo-catalysis Using Titanium Dioxide Nanotube Layers. *Journal of Photochemistry and Photobiology*, 199, 250-254.
- [41] **Surface roughness.** (n.d.). In *Wikipedia*. Date retrieved: 12.12.2011, address: [http://en.wikipedia.org/wiki/Surface\\_roughness](http://en.wikipedia.org/wiki/Surface_roughness)
- [42] **Çolak, Z.** (2008). Anodik Oksidasyon Yöntemi ile Üretilen Titanyum Oksit Nanotüplerin Hidrojen Algılama Özelliklerinin İncelenmesi. *M.Sc. Thesis*, Gebze Institute of Technology, Turkey.



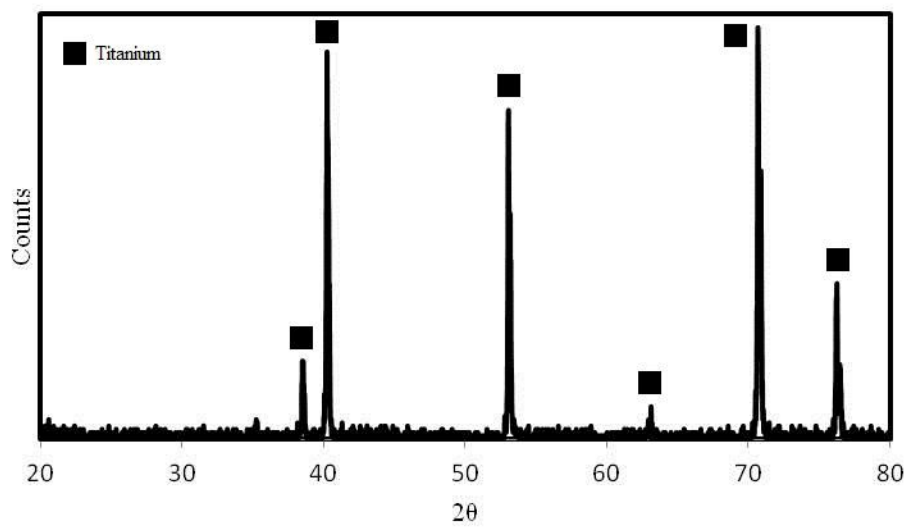
## **APPENDICES**

### **APPENDIX A.1 : XRD Patterns**

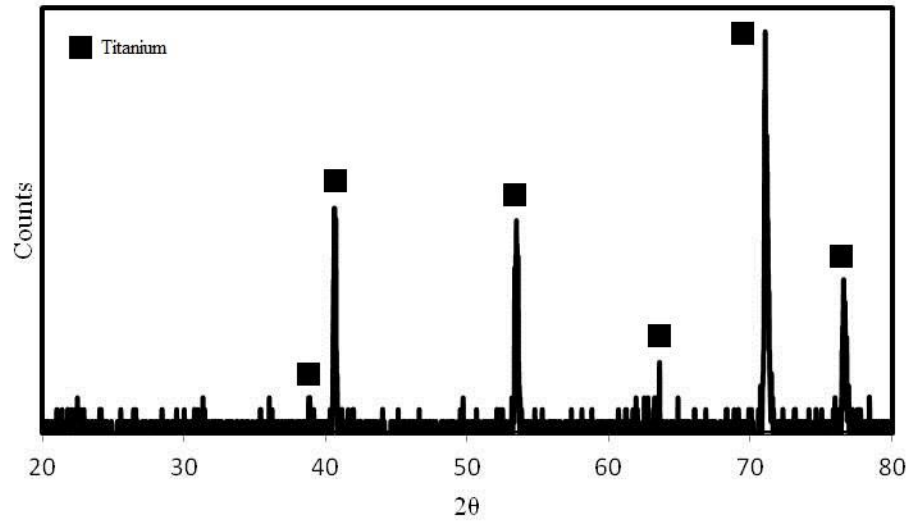
## APPENDIX A.1



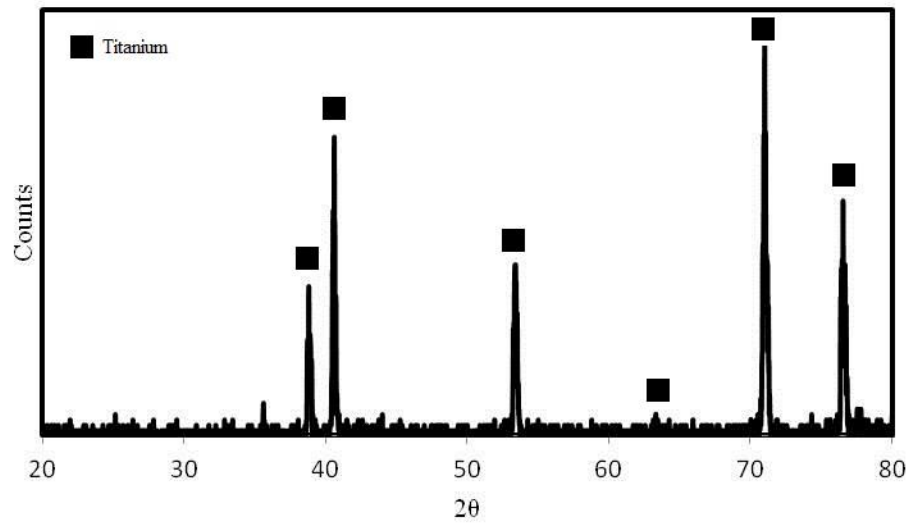
(a)



(b)

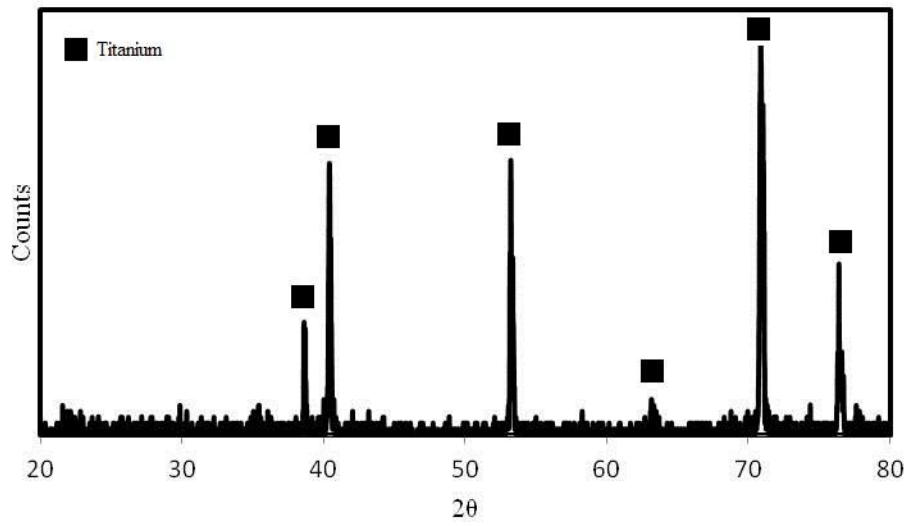


(c)

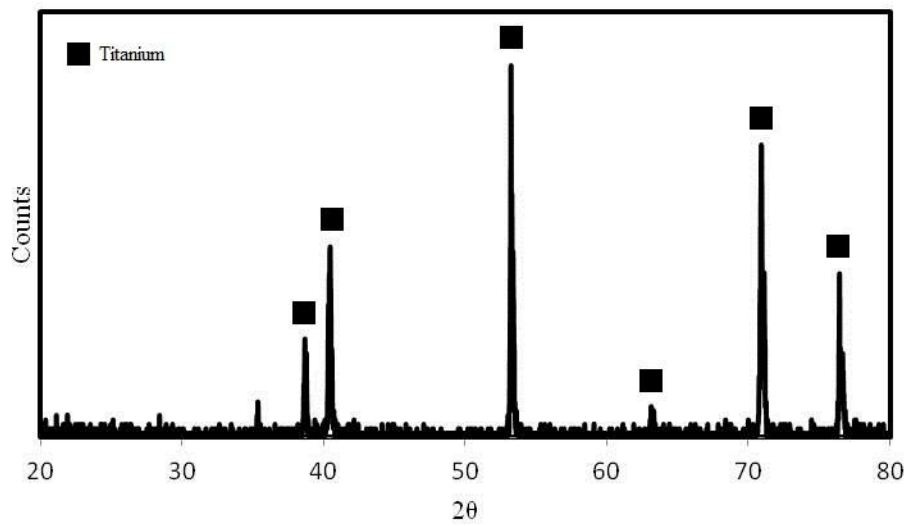


(d)

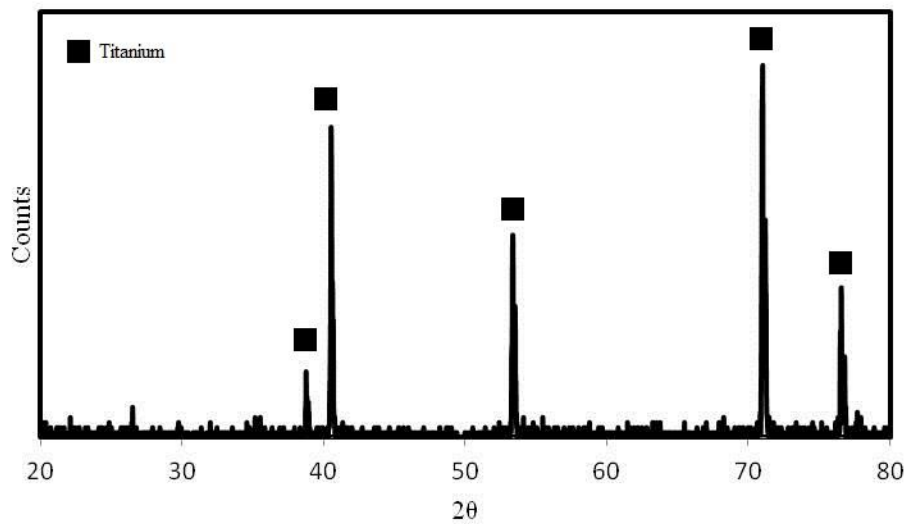
**Figure A.1:** XRD patterns of unannealed samples anodized at 10V with anodization time: (a) 5 minutes, (b) 10 minutes, (c) 20 minutes, (d) 40 minutes.



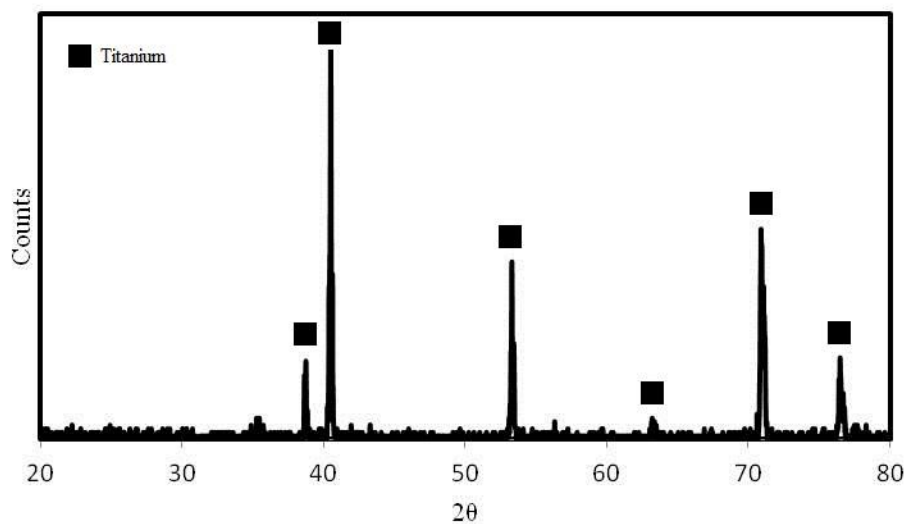
(a)



(b)

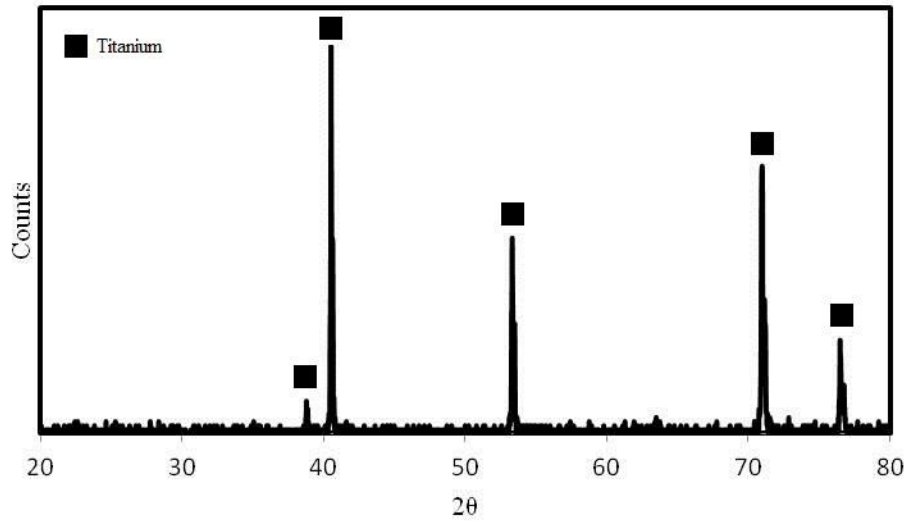


(c)

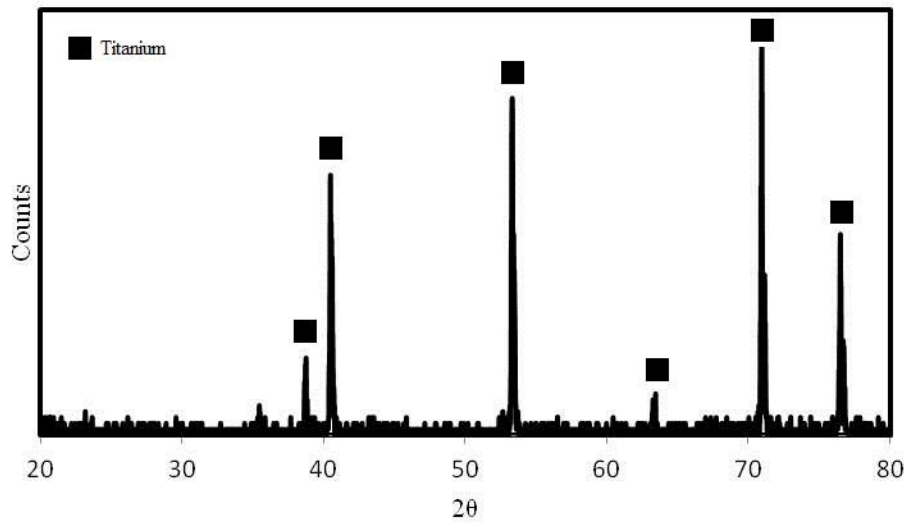


(d)

**Figure A.2:** XRD patterns of unannealed samples anodized at 20V with anodization time: (a) 5 minutes, (b) 10 minutes, (c) 20 minutes, (d) 40 minutes.

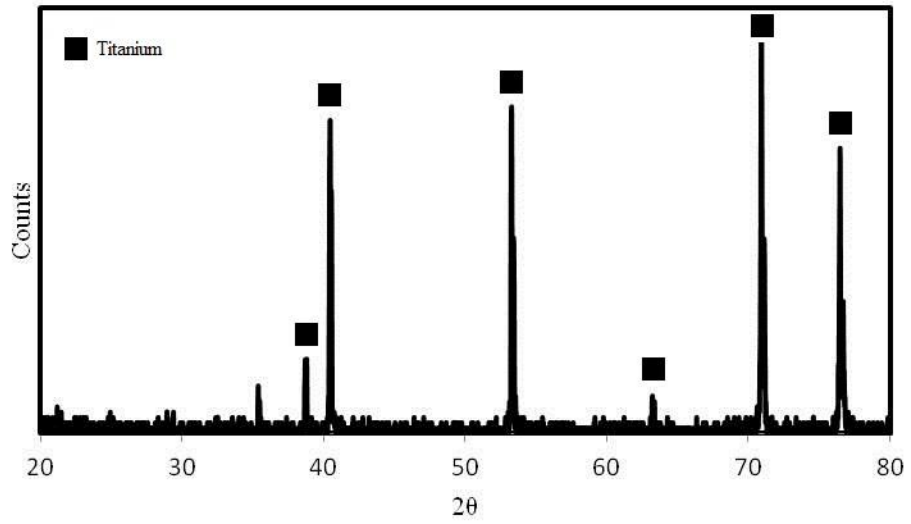


(a)

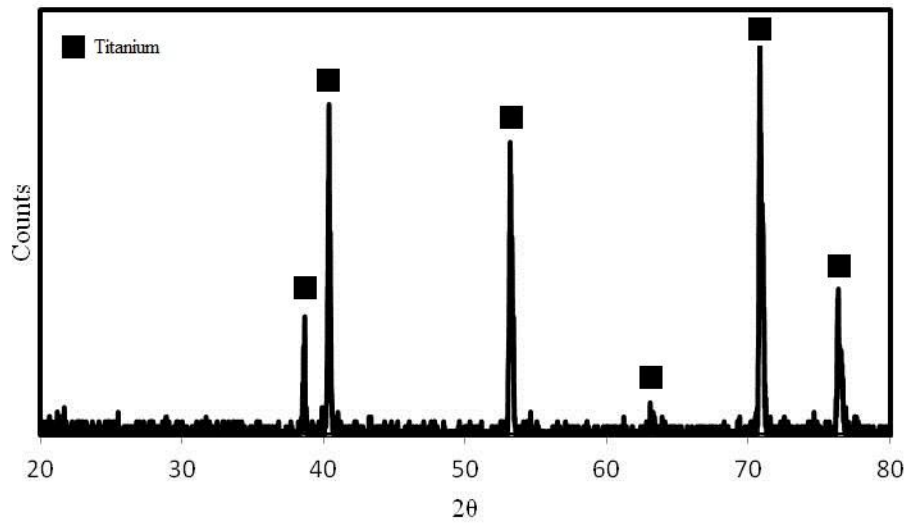


(b)





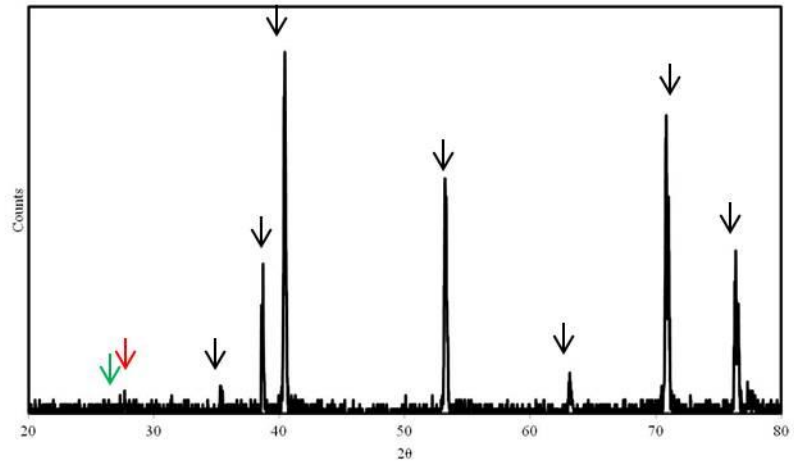
(c)



(d)

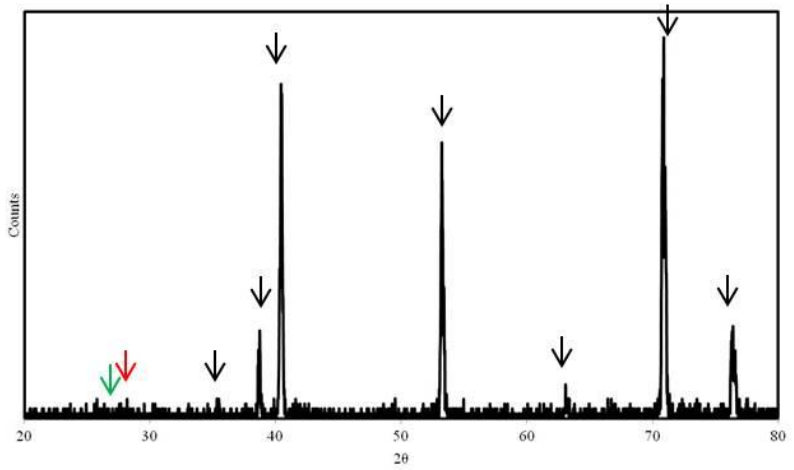
**Figure A.3:** XRD patterns of unannealed samples anodized at 40V with anodization time: (a) 5 minutes, (b) 10 minutes, (c) 20 minutes, (d) 40 minutes.

↓ Anatase  
↓ Rutile  
↓ Titanium



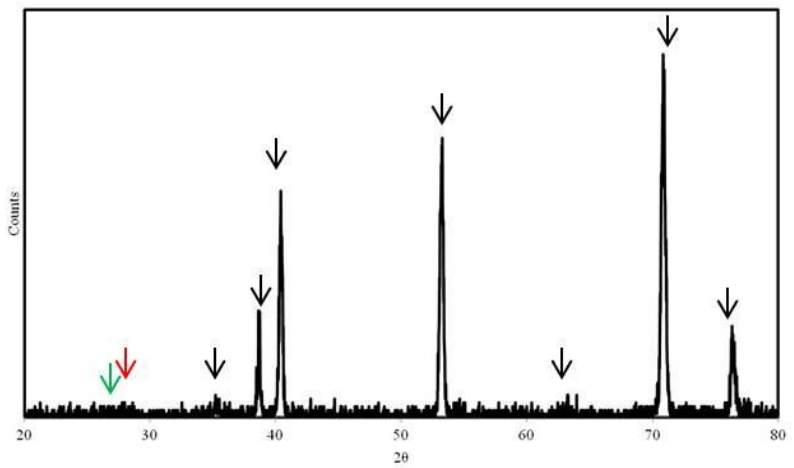
(a)

↓ Anatase  
↓ Rutile  
↓ Titanium



(b)

↓ Anatase  
↓ Rutile  
↓ Titanium



(c)

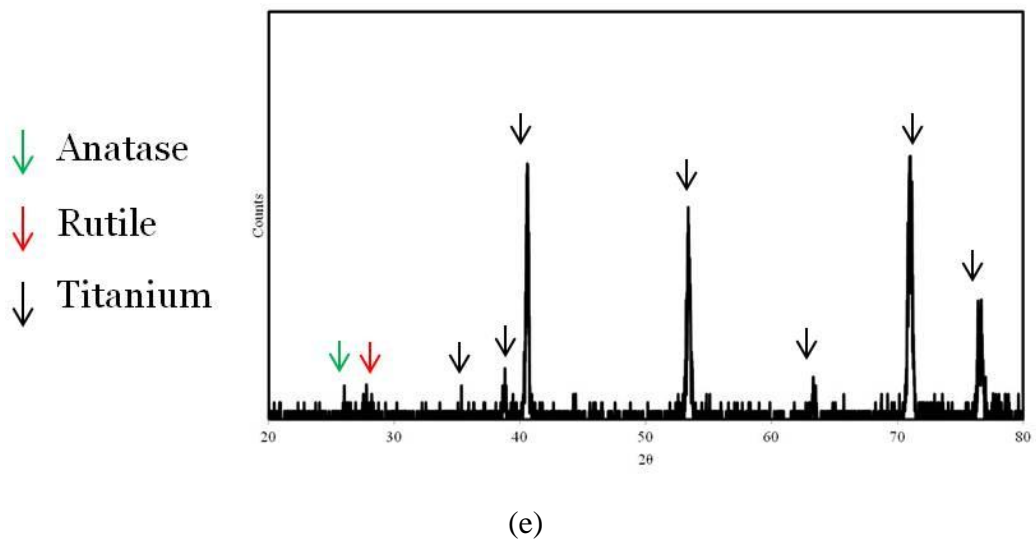
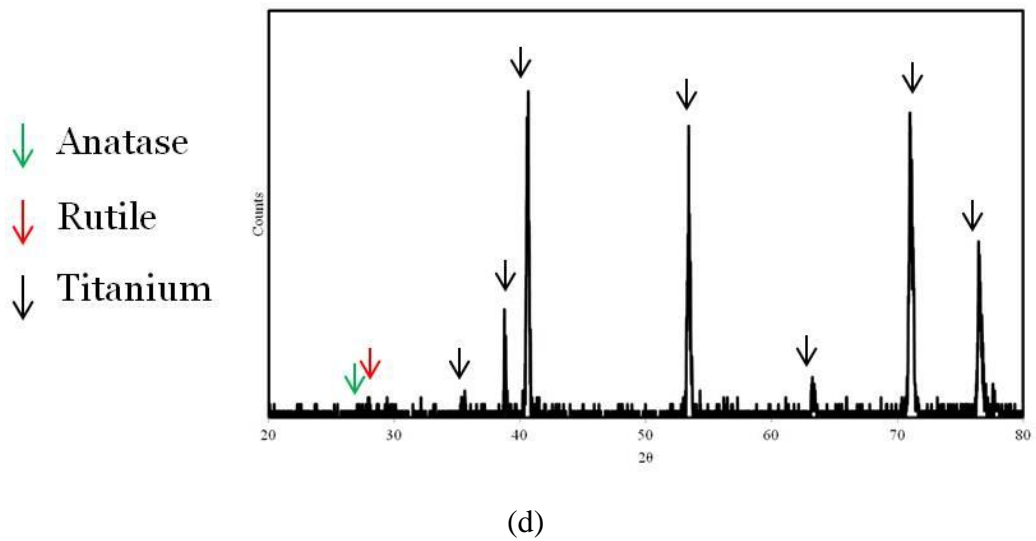
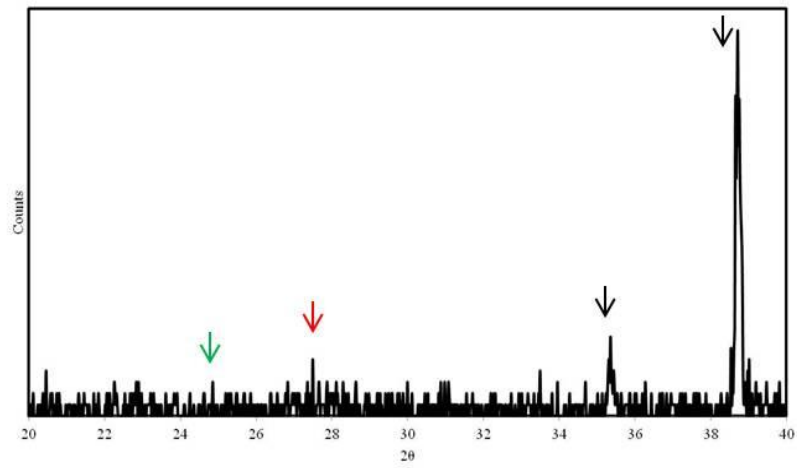


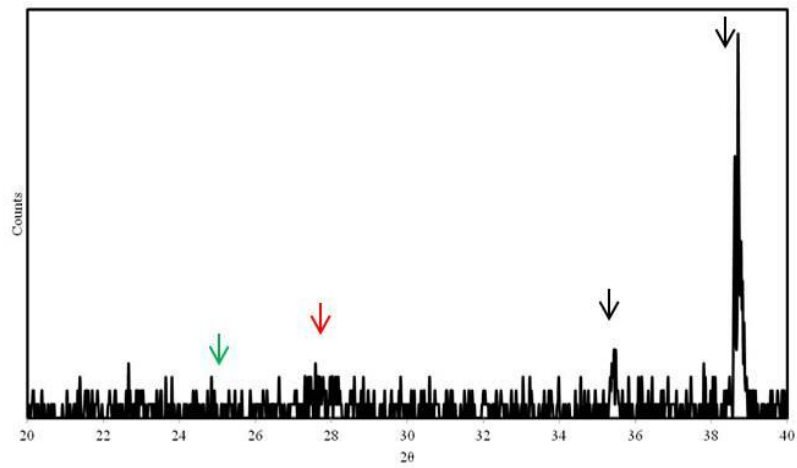
**Figure A.4:** XRD patterns of samples annealed at 480°C. Annealing time: (a) 1 hour, (b) 2 hours, (c) 4 hours, (d) 8 hours, (e) 24 hours.

↓ Anatase  
↓ Rutile  
↓ Titanium



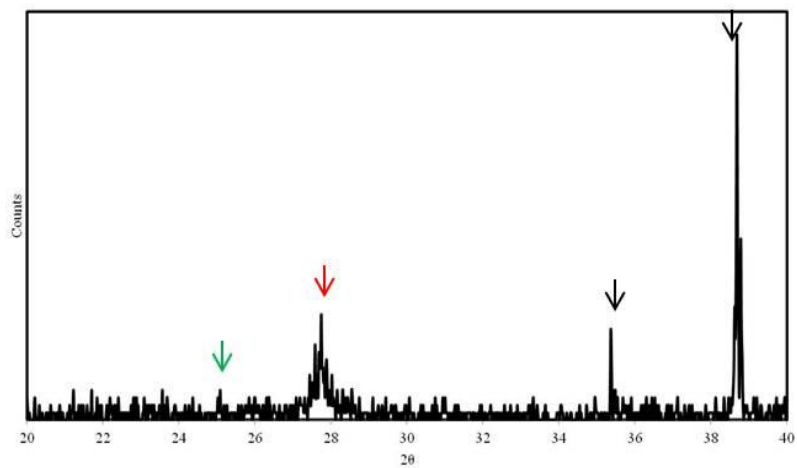
(a)

↓ Anatase  
↓ Rutile  
↓ Titanium

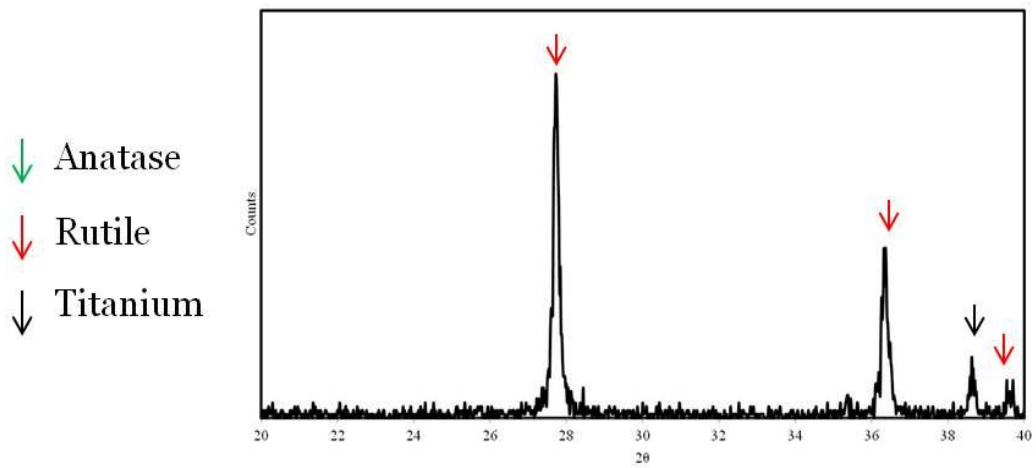


(b)

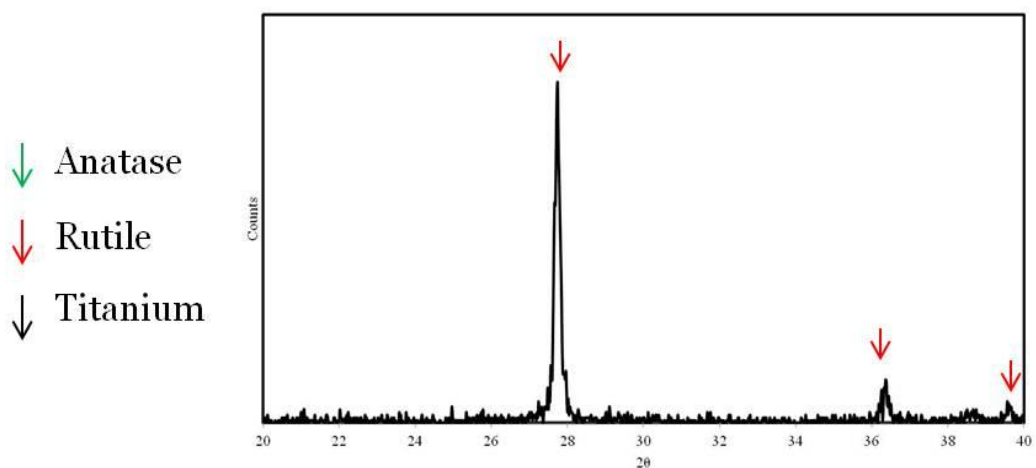
↓ Anatase  
↓ Rutile  
↓ Titanium



(c)



(d)



(e)

**Figure A.5:** XRD patterns of samples annealed at (a) 400°C for 1 hour, (b) 500°C for 1 hour, (c) 600°C for 1 hour, (d) 600°C for 60 hours, (e) 700°C for 1 hour.



## **CURRICULUM VITAE**

**Name Surname:** Timur ÖZTÜRK

**Place and Date of Birth:** Eminönü – İSTANBUL / 03.10.1987

**Address:** Denizköşkler M. Reşitpaşa C. Bülbül S. No: 18/3  
Avcılar - İSTANBUL

**E-Mail:** ozturkti@itu.edu.tr

**B.Sc.:** Istanbul Technical University  
Metallurgical and Materials Engineering (2005 – 2009)